

# Granovskii-Zhedanov Scar of XYZ Spin-chain: Modern Algebraic Perspectives and Realization in Higher Dimensional Lattices

Dhiman Bhowmick<sup>1,\*</sup> and Wen Wei Ho<sup>1,2,†</sup>

<sup>1</sup>*Department of Physics, National University of Singapore, Singapore 117551*

<sup>2</sup>*Centre for Quantum Technologies, National University of Singapore, 3 Science Drive 2, Singapore 117543*

(Dated: July 22, 2025)

In a work by Granovskii and Zhedanov, a surprising scar state exhibiting zero entanglement and long periodicity was discovered in the XYZ spin chains—remarkably, nearly three decades before the concept of many-body scars became a subject of active research. Despite its significance, this state has largely gone unnoticed within the physics community. In this study, we uncover the origin of the Granovskii-Zhedanov (GZ) scar within the framework of the modern understanding of quantum many-body scars. We demonstrate that the scar subspace can be effectively described using the standard spectrum-generating algebra (SGA) framework, as well as through a group-theoretical formulation of the Hamiltonian. This description, however, is applicable only in the XXZ limit, where a quasi- $U(1)$  symmetry exists within the scar subspace. In contrast, the absence of such quasi- $U(1)$  symmetry for the GZ scar subspace restricts the applicability of these standard formulations. We propose two alternative techniques to overcome this—approximated SGA and generalized SGA—which construct and describe the scar subspace in the XYZ case. Using these approaches, we are able to identify the scar subspaces and elucidate their interrelationships. We further explore the possibility of constructing lattice-independent GZ scars in higher-dimensional uniform spin-exchange systems with centrosymmetry, using graphical rules developed for GZ scar construction. Our results indicate that lattice-independent GZ scars cannot be supported on uniform lattices with odd coordination numbers or plaquettes with an odd number of edges, while uniform lattices featuring even coordination numbers and even-edged plaquettes can host such lattice-independent scars in specific scenarios. Remarkably, if certain bonds retain the full  $SU(2)$  symmetry of the spin-exchange interaction—thereby breaking the spatial uniformity of the lattice—lattice-independent GZ scars can still emerge in systems with odd coordination numbers or plaquettes with an odd number of edges.

## I. INTRODUCTION

The Eigenstate Thermalization Hypothesis (ETH) is a cornerstone in quantum many-body dynamics [1–4]. ETH has long been thought to describe the properties of all excited states in the middle of the spectrum of any generic quantum many-body system [5–9]. Although the formulation of ETH appears to be generic, it is nevertheless a hypothesis, and thus, it is natural to ask whether potential counterexamples exist. Many-body localization [10, 11] and integrable systems strongly violate the ETH, whereas quantum many-body scars (QMBS) constitute a weak violation, as only an exponentially small subset of states in the Hilbert space deviate from it.

The first many-body scar is observed in a Rydberg atom quantum simulator, where the simplistic product states  $\mathbb{Z}_2$  revealed unexpected long-lived revivals of the state [12, 13]. These revivals were linked to a small subset of non-thermal eigenstates QMBS of the non-integrable PXP model used to describe the system. As a result, the information stored in the system remains intact without dissipating through thermalization, making it a promising candidate for applications in quantum information and quantum computing [14, 15]. Subsequently, numerous studies emerged, aiming to understand the

origin of QMBS and explore ways to stabilize them within the paradigmatic PXP model [16–22]. The current knowledge of this phenomena is not only limited to the PXP chain, variety of other interesting systems have also been identified, including the 1D transverse field Ising model [23, 24], the fermionic Hubbard model [25–28], quantum Hall systems [29, 30], fracton topological ordered systems [31, 32], AKLT spin chain [33–36], the spin-1 XY model [37, 38], frustrated spin systems [39, 40] and more [41, 42].

Spin systems, in particular, have long been a central focus in the study of exotic phenomena in many-body physics, owing to their straightforward implementation in both condensed matter systems [43–49] and quantum simulators [50–54]. Interestingly, in spin- $S$  XXZ chain, there exists a scar state—known as a helical scar state—with a spatial periodicity larger than that of the system itself. Experimentally, this state has also been realized in cold atom systems for the spin-1/2 XXZ chain, where it has been identified as a Bethe-phantom state [53–55]. The helical state—though not necessarily a scar state—has been a central focus of numerous studies due to its anomalous dynamical behavior [56–61]. Surprisingly, an adiabatically equivalent state also exists in the spin- $S$  XYZ chain, despite the absence of a  $U(1)$  symmetry. Originally introduced by Granovskii and Zhedanov, this scar state is hereafter referred to as the Granovskii-Zhedanov (GZ) scar [62, 63]. Although the work of Granovskii and Zhedanov was contemporaneous

\* dhiman@nus.edu.sg

† wenweiho@nus.edu.sg

with Heller's introduction of quantum scars in the single-particle context [64], the concept of many-body scars did not emerge in the literature until nearly three decades later. This naturally prompts the question of how a scar state of such striking character, yet long overlooked by the physics community, fits into the contemporary understanding of many-body scar phenomena. This state has only recently been reintroduced in our work [65], as well as independently in a study by Mingchen et al., [66]. However, many fundamental questions about the nature and structure of this state remain unresolved, that we aim to address in the present study.

In this study, we analyze the underlying scar subspace associated with the GZ scar state. This subspace exhibits a thermodynamically large degeneracy—that is, the number of degenerate states increases with the size of the system. While standard frameworks such as spectrum-generating algebra (SGA) and group-theoretical constructions of the Hamiltonian can describe the scar subspace, their applicability is restricted to the XXZ limit, where a quasi- $U(1)$  symmetry is present [28, 35, 41, 67–69]. In the XXZ regime, the GZ scar state becomes a more well-known helical state [52–54, 56–61, 70], and we demonstrate that the resulting helical scar subspace is equivalent to a set of bosonic  $\zeta$ -states. However, in the XYZ limit, the absence of quasi- $U(1)$  symmetry renders these standard formalisms inapplicable. To address this, we introduce two alternative approaches—*approximated*-SGA and *generalized*-SGA—to construct and understand the GZ scar subspace beyond the XXZ limit. These approaches not only facilitate the characterization of the GZ scar subspace but also uncover rich internal structures and interrelations among scar subspaces. Notably, we find that the span of the GZ scar subspace with a particular helicity is larger than that of the helical scar subspace with the same helicity. This indicates that the GZ scar state is not merely a deformation of the helical scar state within a given helical sector. Consequently, the standard SGA formalism—applicable in the helical case—cannot be smoothly connected to the GZ scar subspace. Nevertheless, the GZ scar subspace exhibits a significant overlap with the corresponding helical scar subspace, suggesting that the GZ scar state can still be well approximated using the helical scar basis.

We further demonstrate that the presence of the GZ scar state is not limited to one-dimensional XYZ spin chains, but can also arise in higher-dimensional lattice systems. Felix et al. [61] show that the helical scars of XXZ models can be constructed in arbitrary-dimensional lattices using simple graphical rules: the vertex rule and the circuit rule. These laws are also applicable within the XYZ limit, with slight modifications. Applying these rules, we identify the classes of uniform lattices in two dimensions with centrosymmetric spin-exchange (CSSE) interactions that support the construction of lattice-independent GZ scar states, where lattice-independent means that the choice of the parameters of the scar state is independent of the lattice geometry

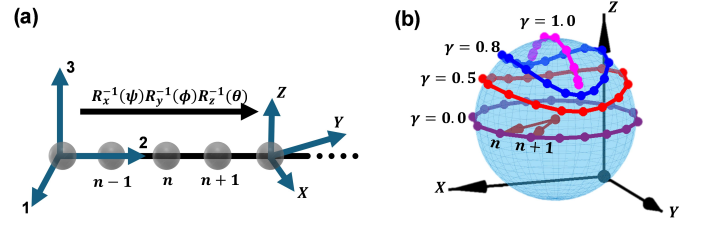


FIG. 1. (a) Transforming a generic NN CSSE Hamiltonian 1 to an XYZ Hamiltonian 2, via  $SO(3)$  rotations ( $R_x(\psi)$ ,  $R_y(\phi)$ ,  $R_z(\theta)$ ) on the lab frame (1, 2, 3). (b) The Bloch sphere of radius  $S$  represents the Granovskii-Zhedanov scar on a 1D spin chain. The dots on the sphere denote spin sites, while the arrows extending from the origin to each dot represent the spins.

and solely depends on the system Hamiltonian. We also demonstrate that uniform lattices, which are unsuitable for constructing lattice-independent scars, can still support such states, provided that certain bonds retain the full  $SU(2)$ -symmetric Heisenberg exchange interaction, thereby breaking the spatial uniformity of the system.

## II. OVERVIEW OF GZ SCARS

A centro-symmetric model is one in which inversion symmetry is preserved. A generic centro-symmetric spin exchange (CSSE) Hamiltonian with nearest-neighbor (NN) coupling on a 1D chain can be written as,

$$\begin{aligned} \hat{H} = \sum_n & \left[ J_1 \hat{S}_n^1 \hat{S}_{n+1}^1 + J_2 \hat{S}_n^2 \hat{S}_{n+1}^2 + J_3 \hat{S}_n^3 \hat{S}_{n+1}^3 \right. \\ & + J_{12} \left( \hat{S}_n^1 \hat{S}_{n+1}^2 + \hat{S}_n^2 \hat{S}_{n+1}^1 \right) + J_{13} \left( \hat{S}_n^1 \hat{S}_{n+1}^3 + \hat{S}_n^3 \hat{S}_{n+1}^1 \right) \\ & \left. + J_{13} \left( \hat{S}_n^1 \hat{S}_{n+1}^3 + \hat{S}_n^3 \hat{S}_{n+1}^1 \right) \right], \end{aligned} \quad (1)$$

where (1, 2, 3) represents the orthogonal basis of the lab frame (see Fig. 1(a)). This Hamiltonian can be transformed into the simple 1D XYZ Hamiltonian via a change of reference frame (see Fig. 1(a)),

$$\hat{H} = \sum_n \left[ J_x \hat{S}_n^x \hat{S}_{n+1}^x + J_y \hat{S}_n^y \hat{S}_{n+1}^y + J_z \hat{S}_n^z \hat{S}_{n+1}^z \right]. \quad (2)$$

Appendix A provides a systematic process and detailed explanation of this transformation. Granovskii and Zhedanov show that a periodic product state with periodicity much greater than one unitcell is a quantum manybody scar of 1D XYZ spin chain (see Appendix B),

$$|\Psi_{\pm GZ}\rangle = \hat{\mathcal{R}}_{\pm} |\uparrow\rangle, \quad (3)$$

where, the sign in the subscript + and - denote the GZ scar state with positive and negative helicity respectively. The rotation operators  $\hat{\mathcal{R}}_{\pm}$  for positive or negative helicity

ity is defined as,

$$\begin{aligned}\hat{\mathcal{R}}_{\pm} &= \prod_n \exp(\pm i \hat{S}_n^z \phi_n) \exp(-i \hat{S}_n^y \theta_n) \\ \text{with, } \theta_n &= \cos^{-1} \left( \frac{\langle \hat{S}_n^z \rangle}{S} \right), \quad \phi_n = \tan^{-1} \left( \frac{\langle \hat{S}_n^y \rangle}{\langle \hat{S}_n^x \rangle} \right), \\ \langle \hat{S}_n^x \rangle &= S \alpha \operatorname{cn}(nq, \kappa), \quad \langle \hat{S}_n^y \rangle = S \beta \operatorname{sn}(nq, \kappa), \\ \langle \hat{S}_n^z \rangle &= S \gamma \operatorname{dn}(nq, \kappa),\end{aligned}\quad (4)$$

where  $|\uparrow\rangle$  is a fully-polarized state and (cn, sn, dn) are Jacobi elliptic functions. The parameters  $(q, \kappa)$  are related to the parameters of 1D XYZ Hamiltonian  $(J_x, J_y, J_z)$  as

follows (in the case  $J_y \geq J_x > J_z$ ),

$$\operatorname{dn}(q, \kappa) = \frac{J_x}{J_y}, \quad \operatorname{cn}(q, \kappa) = \frac{J_z}{J_y}, \quad \kappa^2 = \frac{J_y^2 - J_x^2}{J_y^2 - J_z^2}. \quad (5)$$

On the other hand, parameters  $(\alpha, \beta, \gamma)$  are related as,

$$\alpha = \sqrt{1 - \gamma^2}, \quad \beta = \sqrt{1 - \gamma^2 + \kappa^2 \gamma^2}, \quad |\gamma| \leq 1. \quad (6)$$

It is important to note that the parameter  $\gamma$  is independent of the spin system and can therefore be chosen arbitrarily. Consequently, Eq. 3 does not represent a unique scar state but rather an infinite family of scar states which are visualized in Fig. 1(b). Moreover, the scar state Eq. 3 generalizes the scar state of easy-plane 1D XXZ spin chain for an XYZ-type model. For a finite periodic chain of length  $N$ , the only allowed GZ scar states correspond to  $q$ -values of the form  $4pK(\kappa)/N$ , where  $p$  is an integer and  $K(\kappa)$  is the complete elliptic integral of the first kind.

### III. MODERN ALGEBRAIC PERSPECTIVE

A compelling question arises: What is the underlying algebra that leads to the emergence of such a spatially periodic product state as an eigenstate of the XYZ Hamiltonian? Significant progress has been made in understanding scar states very recently, unveiling diverse approaches to their underlying origins. These range from the Shiraishi-Mori construction to group-theoretical formulation of the Hamiltonian [68, 69, 71], as well as insights from spectral analysis and the associated spectrum-generating algebras [28, 35, 42, 67]. This section examines the origin of GZ scars through various lenses, focusing on the spectral properties and the algebraic structure of the Hamiltonian.

The emergence of such a periodic, unentangled scar state is reflected in its spectral degeneracy, as it is formed from a superposition of many finite entangled states with the same energy, drawn from different symmetry sectors. To demonstrate this, we perform exact diagonalization on the Hamiltonian 2 for a 1D periodic chain of length  $N$  and calculate the degeneracy  $\mathcal{D}$  at the energy level corresponding to the GZ scar (see Appendix. C for more details),

$$\begin{aligned}E_{GZ} &= NS^2 \operatorname{cn}(q, \kappa) \operatorname{dn}(q, \kappa) \\ &+ k^2 S^2 \operatorname{sn}^2(q, \kappa) \sum_n \operatorname{sn}(nq, \kappa) \operatorname{sn}(nq + q, \kappa).\end{aligned}\quad (7)$$

The degeneracy  $\mathcal{D}$  as a function of  $q$ -value for various system sizes and spin values is shown in Fig. 2(c). Except for the spin-1/2 cases and the special  $q$ -values that are integer multiples of  $K(\kappa)$ , the degeneracy  $\mathcal{D}$  follows a well-defined mathematical form:  $\mathcal{D} = 4NS$ . The deviations

in degeneracy for the spin-1/2 XYZ model arise due to its integrability. Additionally, the exceptions also occur at  $q$ -values that are integer multiples of  $K(\kappa)$ . At these  $q$ -values, the model reduces to either the XY model or the isotropic Heisenberg model, with ferromagnetic or anti-ferromagnetic Ising interactions. These special cases are not examined in detail in the present study, and we treat the degenerate space as having a degeneracy of  $4NS$ . Next, we address the underlying algebra of the scar subspace and the relations among different scar subspaces.

#### A. XXZ Limit: Helical-scar Subspace

In the XXZ limit the GZ scar state reduces to Helical scar state. The dynamics of helical states—though not necessarily scar states—have long been of central interest in spin models, owing to their anomalous dynamical behavior [56–61] and the relative ease with which they can be realized experimentally [52–54, 70], due to their product state nature. The formation of the Helical scar state can be described based on spectrum generating algebra (SGA). The SGA formulation in the spin- $\frac{1}{2}$  XXZ limit is presented in Ref. [67]. This approach can be generalized to arbitrary higher spin values  $S$ . If  $\hat{\tau}$  is the generator of SGA that generates a tower of scar states from a simple product state like  $|\uparrow\rangle$ , then it must obey (see Appendix. C),

$$[\hat{H}, \hat{\tau}_{\pm}] \left| \mathcal{S}_{\pm H}^{(m)} \right\rangle = \omega \hat{\tau}_{\pm} \left| \mathcal{S}_{\pm H}^{(m)} \right\rangle, \quad (8)$$

where  $\omega$  is the energy spacing between the states  $\left| \mathcal{S}_{\pm H}^{(m)} \right\rangle$  and  $\left| \mathcal{S}_{\pm H}^{(m+1)} \right\rangle$  in scar sub-space. Particularly for the case

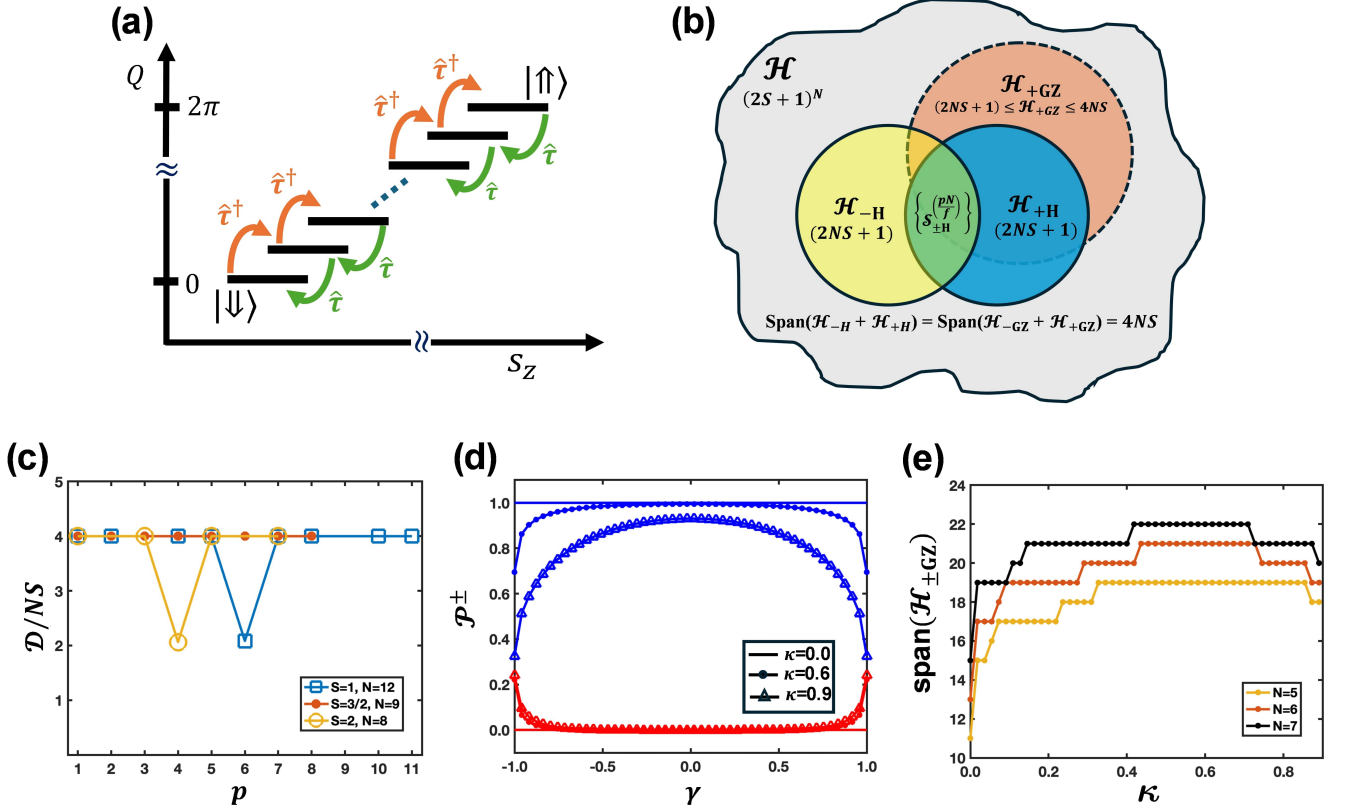


FIG. 2. (a) The tower of scars in the space of translational quantum number  $Q$  and spin quantum number  $s_z$ . (b) The schematic illustrates the span of the Hilbert space along with the scar subspaces. It also provides insight into the relationships and overlaps among the scar subspaces. (c) The degeneracy at the energy of GZ scar as a function of  $q$ -value ( $q = 4pK(\kappa)/N$ ) for various values of spins and system sizes. The degeneracy is generally  $4NS$ , except in the case of spin  $S = 1/2$ , or when  $q$  takes special values that are integer multiples of  $K(\kappa)$ . For these special  $q$ -values, the Hamiltonian turns into either the XY Hamiltonian or the isotropic Heisenberg Hamiltonian with either ferromagnetic or antiferromagnetic Ising interactions. In particular, the value  $\kappa = 0.8$  is used for the numerical simulations. Data points corresponding to  $q$ -values that are odd integer multiples of  $K(\kappa)$  are omitted from the plot for clarity, due to their high degeneracy (approximately 3000). (d) Projection of the GZ scar state with positive helicity onto the spaces of helical scar states—with positive helicity ( $\mathcal{P}^+$ , shown in blue) and negative helicity ( $\mathcal{P}^-$ , shown in red). This reveals that the GZ scar state exhibits a strong overlap with the helical scar subspace of the same helicity, especially in the limit  $\gamma \rightarrow 0$ . The numerical simulations are done for  $S = 1$  and  $N = 7$ . The results are independent of commensurate  $q$ -values ( $q = 4pK(\kappa)/N$ ). (e) The span of GZ scar subspaces with a given helicity is not constant in  $\kappa$ , but rather varies with it. This implies that the standard SGA framework is insufficient for describing the GZ scar subspace, which requires the span to remain constant with  $\kappa$ . Instead, a generalized SGA approach is necessary in such cases. In particular, the numerical simulations are done for spin  $S = 1$ .

of Helical scars, the states are generated as follows,

$$|\mathcal{S}_{\pm H}^{(m)}\rangle = \hat{\tau}_{\pm}^m |\mathcal{S}_H^{(0)}\rangle \quad \text{with} \quad \hat{\tau}_{\pm} = \sum_n e^{\pm i n q} \hat{S}_n^{\pm}, \quad (9)$$

where  $|\mathcal{S}_H^{(0)}\rangle = |\uparrow\rangle$ . The scar states can be further identified using translational and total spin quantum numbers  $Q$  and  $s_z$  respectively,

$$|\mathcal{S}_{\pm H}^{(m)}\rangle = |Q = \pm m q, s_z = NS - m\rangle, \quad (10)$$

thus forming a tower of scars shown in Fig. 2(a). Interestingly, because the tower of scars collapses ( $\omega = 0$ ) to a degenerate energy level, the superposition of such states

results in another scar state. Specifically, the helical scar state in terms of tower states  $|\mathcal{S}_{\pm H}^{(m)}\rangle$  can be represented as,

$$|\psi_{\pm H}\rangle = \sum_{m=0}^M \sqrt{M C_m} \cos^{M-m} \left( \frac{\theta}{2} \right) \sin^m \left( \frac{\theta}{2} \right) |\mathcal{S}_{\pm H}^{(m)}\rangle, \quad (11)$$

where,  $M = 2NS$ . This helical state is identical to the GZ scar in Eq. 3 in the XXZ limit ( $\kappa \rightarrow 0$ ), with  $\phi_n = nq$  and  $\theta_n = \theta$ , up to a global phase factor  $\exp(-iSN(N+1)q/2)$ . Notably, the scar subspace spans a dimension of  $M = 2NS + 1$  for each helicity sectors  $\pm$ . The joint span of the two helicity sectors yields a total dimension of  $4NS$ , which matches the degeneracy of



the GZ scar states, discussed in the beginning of this section. It is noteworthy that although each helicity sector spans a space of dimension  $2NS + 1$ , the total dimension of their joint span is  $4NS$ , since the two states  $|\uparrow\rangle$  and  $|\downarrow\rangle$  are shared between both sectors. Fig. 2(b) schematically shows the helical scar subspace  $\mathcal{H}_{\pm H}$  within the Hilbert space  $\mathcal{H}$ . It is interesting to observe that the helical scar subspaces with opposite helicities share a set of common states, denoted by  $\mathcal{S}_{\pm H}^{(pN/f)}$ , where  $f = 1$  (or  $f = 2$ ) for odd (or even)  $N$ . The states corresponding to  $p = 0$  and  $p = 2Sf$  are the fully polarized states  $|\uparrow\rangle$  and  $|\downarrow\rangle$ , respectively. Whereas, the states with  $0 < p < 2Sf$  are non-orthogonal and are unequally shared between the two helical sectors.

Interestingly, when expressed in terms of Schwinger bosons, the states described in Eq. 9 correspond to the bosonic analogs of the  $\zeta$ -states, described in reference [69]. Thus, the existence of such scar subspace suggests an underlying group-theoretical structure of the XXZ Hamiltonian, which can be expressed in the form  $\hat{H}_0 + \sum_a \hat{O}_a \hat{T}_a$  [68, 69]. This decomposition consists of a simple integrable part,  $\hat{H}_0$ , and a set of generators,  $\hat{T}_a$ , of a group  $G$ , which satisfy the commutation relation  $[\hat{H}_0, \hat{T}_a] = 0$ —or, more generally, may obey a relationship involving the quadratic Casimir of the group, as discussed in Ref. [68]. Additionally,  $\hat{O}_a$  denotes a set of auxiliary operators, which may or may not be constrained by the requirement of preserving the hermiticity of the Hamiltonian. To show such construction of the Hamiltonian, we work in the rotated basis in which the scar subspace defined in Eq. 9 takes form of  $\zeta$ -states as in Ref. [69]. This is done using unitary operator  $\prod_n \exp(inq\hat{S}_n^z)$  (for positive helicity sector) and this rotation simultaneously transforms the Hamiltonian (with  $J_x = J_y$  and  $J_z = \cos(q)$ ),

$$\begin{aligned} \hat{H} = & J_x \cos(q) \sum_n \hat{\mathbf{S}}_n \cdot \hat{\mathbf{S}}_{n+1} \\ & - J_x \sin(q) \sum_n \hat{z} \cdot (\hat{\mathbf{S}}_n \times \hat{\mathbf{S}}_{n+1}). \end{aligned} \quad (12)$$

Using Schwinger-Boson transformation  $\hat{S}_n^+ = \hat{c}_{n,\uparrow}^\dagger \hat{c}_{n,\downarrow}$ ,  $\hat{S}_n^- = \hat{c}_{n,\downarrow}^\dagger \hat{c}_{n,\uparrow}$ ,  $\hat{S}_n^z = \frac{1}{2}(\hat{c}_{n,\uparrow}^\dagger \hat{c}_{n,\uparrow} - \hat{c}_{n,\downarrow}^\dagger \hat{c}_{n,\downarrow})$ , the Hamiltonian transformed into the following group theoretical form,

$$\begin{aligned} \hat{H} = & -\frac{NJ_x S \cos(q)}{2} \\ & + \frac{J_x \cos(q)}{4} \sum_n \left( \hat{c}_{n,n+1} \hat{c}_{n+1,n} + \hat{c}_{n,n+1}^\dagger \hat{c}_{n+1,n}^\dagger \right) \\ & - \frac{iJ_x \sin(q)}{4} \sum_n \left( \hat{O}_{n,n+1}^{(1)} \hat{c}_{n+1,n} - \hat{O}_{n+1,n}^{(1)} \hat{c}_{n,n+1} \right. \\ & \left. + \hat{O}_{n,n+1}^{(2)} \hat{c}_{n+1,n} - \hat{O}_{n+1,n}^{(2)} \hat{c}_{n,n+1} \right), \end{aligned} \quad (13)$$

where, the first term represents  $\hat{H}_0$  and the rest of the terms represent  $\sum_a \hat{O}_a \hat{T}_a$ . The operators are explicitly

given as,

$$\begin{aligned} \hat{\zeta}_{mn} &= \hat{c}_{m\uparrow}^\dagger \hat{c}_{n\uparrow} + \hat{c}_{m\downarrow}^\dagger \hat{c}_{n\downarrow}, \quad \hat{O}_{mn}^{(1)} = \hat{c}_{m\uparrow}^\dagger \hat{c}_{n\uparrow} - \hat{c}_{m\downarrow}^\dagger \hat{c}_{n\downarrow} \\ \hat{\eta}_{mn} &= \hat{c}_{m\uparrow}^\dagger \hat{c}_{n\downarrow} + \hat{c}_{m\downarrow}^\dagger \hat{c}_{n\uparrow}, \quad \hat{O}_{mn}^{(2)} = \hat{c}_{m\uparrow}^\dagger \hat{c}_{n\downarrow} + \hat{c}_{m\downarrow}^\dagger \hat{c}_{n\uparrow} \\ \hat{\varepsilon}_{mn} &= \hat{c}_{m\uparrow}^\dagger \hat{c}_{n\downarrow} - \hat{c}_{m\downarrow}^\dagger \hat{c}_{n\uparrow}, \end{aligned} \quad (14)$$

where  $m \neq n$ . The operators  $\hat{\zeta}$ ,  $\hat{\eta}$ ,  $\hat{\varepsilon}$  can be written as linear combination of  $SU(N)$  generators and annihilates the bosonic  $\zeta$ -states,

$$|m\zeta\rangle = \hat{\tau}'^m |\downarrow\rangle \quad \text{with } \hat{\tau}' = \sum_n \hat{c}_{n\uparrow}^\dagger \hat{c}_{n\downarrow}, \quad (15)$$

$$\text{and } |\downarrow\rangle = \prod_{n=1}^N \hat{c}_{n\downarrow} |0\rangle$$

Comparing Eq. 15 with Eq. 9, it can be observed that the  $\zeta$ -states are orthonormal basis  $|\mathcal{S}_H^{(m)}\rangle$  in a rotated frame. Moreover any operator  $\hat{o}$  that annihilates the  $\zeta$ -state must follow a set of equations,

$$\hat{o}|\downarrow\rangle = 0, [\hat{o}, \hat{\tau}']|\downarrow\rangle = 0, [[\hat{o}, \hat{\tau}'], \hat{\tau}']|\downarrow\rangle = 0, \dots \quad (16)$$

It can be shown that the operators  $\hat{\zeta}$ ,  $\hat{\eta}$  and  $\hat{\varepsilon}$  obey these equations. Moreover, it is noteworthy that, to obtain the group-theoretical form of Eq. 13, we add a locally non-Hermitian term,  $iSJ_x \sin(q) \sum_n (\hat{S}_n^z - \hat{S}_{n+1}^z)$ , to the rotated Hamiltonian Eq. 12. A similar algebraic technique has been employed in the context of generalized helical scar states for XXC models [60]. This transformation modifies the Hamiltonian such that its local terms become able to annihilate the scar state. Furthermore, the existence of such an elegant scar-subspace structure is due to the quasi- $U(1)$  symmetry of the scar-subspace [72]. The quasi- $U(1)$  symmetry can be understood by introducing a magnetic field term in the  $z$ -direction, which generates equally spaced scar states forming a tower of scars. For the XXZ model, the quasi- $U(1)$  symmetry coincides with the true symmetry of the Hamiltonian. In general, however, this correspondence does not hold.

## B. XYZ Case: GZ-scar Subspace

In contrast to the XXZ limit, determining the scar subspace of the XYZ Hamiltonian presents significant challenges. These stem, in part, from either the lack of a quasi- $U(1)$  symmetry or the difficulty in identifying such a symmetry of the scar subspace. Thus, rather than relying on the conventional description of the scar subspace, we explore it through several alternative approaches. We provide *approximated*-SGA and *generalized*-SGA approach to describe the scar subspace of GZ-scar. In the *approximated*-SGA approach, we show how perturbatively deforming the scar-subspace in XXZ limit still describes the scar-subspace in XYZ limit approximately.

Whereas, in the *generalized*-SGA approach, we generalize the standard SGA description described by Eq. 8 and describe the way to generate GZ-scar subspace.

First, we investigate whether the GZ scar state with a particular helicity and  $q$ -value ( $q = 4pK(\kappa)/N$ ) can still be constructed using the helical-scar subspace with same helicity and the corresponding  $q$ -value ( $q_0 = 2p\pi/N$ ) in the  $\kappa \rightarrow 0$  limit. To address this, we evaluate the projection of the GZ scar state with positive helicity onto the corresponding helical scar subspace, as follows,

$$\begin{aligned} \mathcal{P}^+ &= \sum_{m=0}^{2NS} \left| \langle \Psi_{+GZ} | \mathcal{S}_{+H}^{(m)} \rangle \right|^2, \\ \mathcal{P}^- &= \sum_{\substack{m=1 \\ m \neq \frac{N}{2}}}^{2NS-1} \left| \langle \Psi_{+GZ} | \mathcal{S}_{-H}^{(m)} \rangle \right|^2, \end{aligned} \quad (17)$$

where the  $q$ -values used for  $|\Psi_{+GZ}\rangle$  and  $|\mathcal{S}_{\pm H}^{(m)}\rangle$  are  $q(\kappa) = 4pK(\kappa)/N$  and  $q_0 = q(0) = 2p\pi/N$  respectively. Moreover, the summation for  $\mathcal{P}^-$  excludes some states  $|\mathcal{S}_{\pm H}^{(\frac{N}{2})}\rangle$  with negative helicity, because of finite overlap of these states with the helical-scar subspace with positive helicity, as schematically demonstrated in Fig. 2(b). The projections  $\mathcal{P}^\pm$  are plotted as a function of  $\gamma$  for different values of  $\kappa$  in Fig. 2(d). It is interesting to observe that the GZ scar state with a given helicity exhibits a substantial overlap with the helical scar subspace of the same helicity, with the overlap becoming strongest in the  $\gamma \rightarrow 0$  limit. This overlap of two scar subspaces is also indicated schematically in Fig. 2(b).

Thus, there must exist a perturbative description of the GZ scar states in terms of the SGA states defined in Eq. 9, which describe the helical scar subspace. We refer to this method as the approximated SGA approach. We begin by performing a perturbative expansion of the XYZ Hamiltonian as a function of  $\kappa$ , as follows,

$$\begin{aligned} \hat{H} &= \sum_n \left[ \text{dn}(q, \kappa) \hat{S}_n^x \hat{S}_{n+1}^x + \hat{S}_n^y \hat{S}_{n+1}^y + \text{cn}(q, \kappa) \hat{S}_n^z \hat{S}_{n+1}^z \right] \\ &= \hat{H}_0 + \kappa^2 \hat{H}_1 \end{aligned} \quad (18)$$

where,

$$\begin{aligned} \hat{H}_0 &= \sum_n \left[ \hat{S}_n^x \hat{S}_{n+1}^x + \hat{S}_n^y \hat{S}_{n+1}^y + \cos(q_0) \hat{S}_n^z \hat{S}_{n+1}^z \right], \\ \hat{H}_1 &= -\frac{\sin^2(q_0)}{2} \sum_n \left[ \hat{S}_n^x \hat{S}_{n+1}^x + \frac{\cos(q_0)}{2} \hat{S}_n^z \hat{S}_{n+1}^z \right], \end{aligned} \quad (19)$$

where  $q(\kappa) = 4pK(\kappa)/N$  and  $q_0 = q(0) = 2p\pi/N$ . The first-order perturbation theory in  $\kappa^2$  gives the deformed scar-subspace as,

$$|\mathcal{S}'_{\pm GZ}{}^{(m)}\rangle = \left(1 - \kappa^2 \hat{H}_0^{-1} \hat{H}_1\right) |\mathcal{S}_{\pm H}^{(m)}\rangle. \quad (20)$$

However, this method of deriving the perturbed scar state is numerically challenging, as it requires computing the inverse of the many-body Hamiltonian  $\hat{H}_0$ . While this inversion is straightforward for a non-interacting Hamiltonian, it becomes computationally intractable in the interacting many-body case for large system sizes. As a result, conventional perturbation theory is not well-suited for identifying the deformed many-body scar subspace. Surprisingly, we find that the following deformed generator is capable of reproducing the spectrum with the same accuracy as first-order perturbation theory Eq. 20,

$$|\mathcal{S}'_{\pm GZ}{}^{(m)}\rangle = (\hat{\tau}'')^m |\mathcal{S}_{\pm H}^{(0)}\rangle, \quad \hat{\tau}'' = \sum_n e^{iq_n} \hat{S}_n^-, \quad (21)$$

where,  $q_n = \tan^{-1}(\text{sc}(nq, \kappa))$

The GZ-scar can be approximately reconstructed using these perturbed states in place of the unperturbed states  $\mathcal{S}^{(m)}_{\pm H}$  in Eq. 11 and  $\theta = \cos^{-1} \gamma$ . The approximation performs well as  $\gamma \rightarrow 0$ , whereas it becomes less accurate in the limit  $\gamma \rightarrow 1$ . This behavior arises because, for  $\gamma \rightarrow 0$ , the GZ scar state with a given helicity has a large overlap with the corresponding helical scar subspace as shown in Fig. 2(d). However, as will be shown next, the span of the GZ scar subspace with a given helicity is significantly larger than that of the helical scar subspace with the same helicity. This mismatch in dimensionality leads to reduced accuracy of the approximation in the  $\gamma \rightarrow 1$  limit.

Finally, we introduce the *generalized*-SGA approach to generate a GZ-scar subspace exactly. In the case of *generalized*-SGA, a given set of operators  $\{\hat{\mathcal{T}}^{(p)} | p \in \mathbb{W}\}$  (with  $\mathbb{W}$  being the set of whole number) generates the scar subspace from a common reference state (which may or may not be the part of scar subspace), if it satisfies the generalized version of the SGA relation Eq. 8, given as,

$$[\hat{H}, \hat{\mathcal{T}}^{(p)} (\hat{\mathcal{T}}^{(m)})^*] |\mathcal{S}^{(m)}\rangle = \omega_{pm} \hat{\mathcal{T}}^{(p)} (\hat{\mathcal{T}}^{(m)})^* |\mathcal{S}^{(m)}\rangle, \quad (22)$$

where  $\omega_{pm}$  is the difference between the energies of  $p$ -th and  $m$ -th scar states. Moreover,  $(\hat{\mathcal{T}}^{(m)})^*$  represents the inverse ladder operation corresponding to the operator  $(\hat{\mathcal{T}}^{(m)})$  in the scar subspace, which does not necessarily be an inverse of  $(\hat{\mathcal{T}}^{(m)})$ . It is worth noting that if  $\hat{\mathcal{T}}^{(p)} = (\hat{\tau})^p$ , then substituting  $p = m + 1$  reduces the generalized-SGA expression, Eq. 22, to the standard SGA expression, Eq. 8. If scar subspace is degenerate, such as the GZ scar subspace, we have  $\omega_{pm} = 0$ . A set of rotation operators for different values of  $\gamma$  forms a *generalized*-SGA,  $\{\hat{\mathcal{T}}^{(p)} = \hat{\mathcal{R}}_\pm(\gamma_p)\}$  for GZ scars. However, this set is not unique; a set can also be constructed using a small- $\gamma$  expansion of the rotation operators, as shown in the Appendix. C Moreover, the resulting operator set does

not necessarily generate an orthonormal set of states. Nonetheless, an orthonormal basis can be obtained by applying the Gram–Schmidt procedure. We examine the span of the GZ scar subspace by generating a set of GZ scar states using a set of rotation operators  $\{\hat{\mathcal{R}}_{\pm}(\gamma_p)\}$  and computing the rank of the matrix they form. As shown in the Fig. 2(e), the dimension of the GZ scar subspace with a particular helicity varies with  $\kappa$ , ranging between  $2NS + 1 \leq \text{span}(\mathcal{H}_{\pm\text{GZ}}) \leq 4NS$ . This variation indicates that the standard SGA framework—which assumes a fixed scar subspace dimension—may not adequately describe the GZ scar across all  $\kappa$  values. Therefore, a *generalized*-SGA interpretation is required for GZ scar subspace with a particular helicity.

Finally, we like to review on other alternative approaches for generating scar subspace in the context of GZ scar. In the XXZ limit the scar states reside within an  $SU(2)$  subspace of the full Hilbert space, as the generator of the scar states  $\hat{\tau}$  is an  $SU(2)$  generator. It is reasonable to think that in the XYZ limit, the  $SU(2)$  scar subspace deforms into a  $U(1)$  subspace, and thus the generator must be deformed. However, this must not be the case as the span of the scar subspace in each helicity sector larger for GZ scar compared to helical scars. Furthermore, we verified that the deformation operators constructed in the reference [73], which reduce the  $SU(2)$  subspace to a  $U(1)$  subspace, do not work in the case of GZ scar (see Appendix. C for more details). Additionally, there are recent approaches to systematically construct scar subspaces by *Fock space caging* [74, 75]. This systematic approach, however, is limited to Hamiltonians with chiral or particle-hole symmetry, which is absent in the case of the XYZ Hamiltonian.

#### IV. HIGHER-DIMENSIONAL REALIZATIONS

In this section, we describe how GZ scar states can be realized in higher-dimensional systems, specifically for two-dimensional lattices. In higher dimensions, GZ scar states can, in principle, exist on any lattice. However, their realization typically requires the Hamiltonian to be finely tuned to specific parameters, making such cases of limited practical interest. Therefore, rather than constructing a finely tuned Hamiltonian in higher dimensions for a given GZ scar state, we consider a more relevant question: Given a generic spin-exchange Hamiltonian on a specific two-dimensional lattice that respects certain symmetries, can a GZ scar state emerge as an eigenstate of that system? To address this, we introduce a set of graphical rules. Based on these rules, we classify the types of lattices that are suitable for realizing GZ scar states.

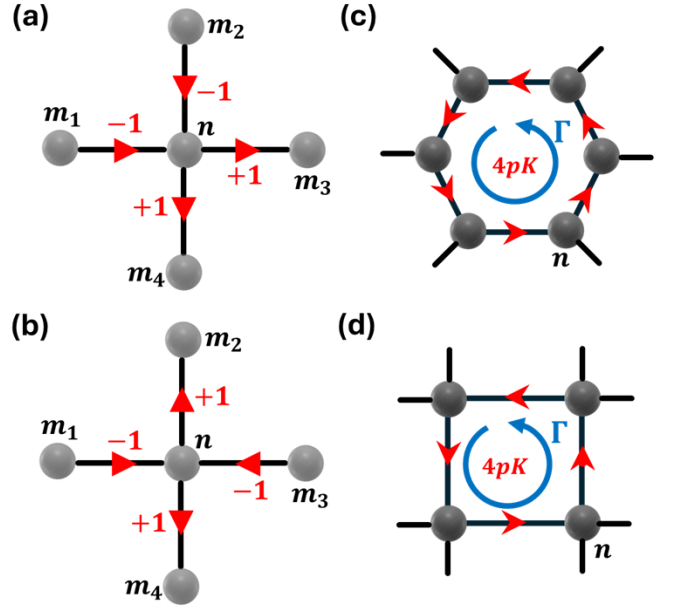


FIG. 3. The visual representations of the vertex rule (a), (b) and the circuit rule (c), (d). The numbers in red and the directions with red arrowheads represent the values of  $\sigma_{nm}$  associated with the edges. Figures (a) and (b) illustrate that the number of ingoing and outgoing arrows from vertex  $n$  is equal, thereby preserving the vertex rule. Figures (c) and (d) demonstrate that along the circuit  $\Gamma$ , the change in variable  $q_n$  in Eq. 24 is  $4pK(\kappa)$ , where  $n$  is an integer.

#### A. Graphical Rules

The scar state can be naturally extended to two or more dimensions by using graphical rules. Inspired by Felix et al. [61], we introduce two graphical rules for constructing scar states on arbitrarily directed simple graphs, where spins at each vertex interact through a CSSE interaction. As described in Sec. II, as well as in the Appendix. A and Fig. 1(a), a specific rotation in the reference frame transforms this kind of Hamiltonian into XYZ form. Without loss of generality, we consider the XYZ Hamiltonian of the following form,

$$\hat{H} = J \sum_{n \sim m} \left[ \text{dn}(q, \kappa) \hat{S}_n^x \hat{S}_m^x + \hat{S}_n^y \hat{S}_m^y + \text{cn}(q, \kappa) \hat{S}_n^z \hat{S}_m^z \right], \quad (23)$$

where the summation is over the adjacent vertices. A scar state of this Hamiltonian is a product state of spins pointing in a certain direction such that the spins on adjacent vertices  $n$  and  $m$ ,

$$\begin{aligned} \langle \hat{S}_n^x \rangle &= \alpha S \text{cn}(q_n, \kappa), \quad \langle \hat{S}_m^x \rangle = \alpha S \text{cn}(q_n - \sigma_{nm} q, \kappa), \\ \langle \hat{S}_n^y \rangle &= \beta S \text{sn}(q_n, \kappa), \quad \langle \hat{S}_m^y \rangle = \beta S \text{sn}(q_n - \sigma_{nm} q, \kappa), \\ \langle \hat{S}_n^z \rangle &= \gamma S \text{dn}(q_n, \kappa), \quad \langle \hat{S}_m^z \rangle = \gamma S \text{dn}(q_n - \sigma_{nm} q, \kappa), \end{aligned} \quad (24)$$

where  $(\alpha, \beta, \gamma)$  are defined in Eq. 6 and  $\sigma_{nm}$  is binary number  $\pm 1$  associated with each edge. The state corre-

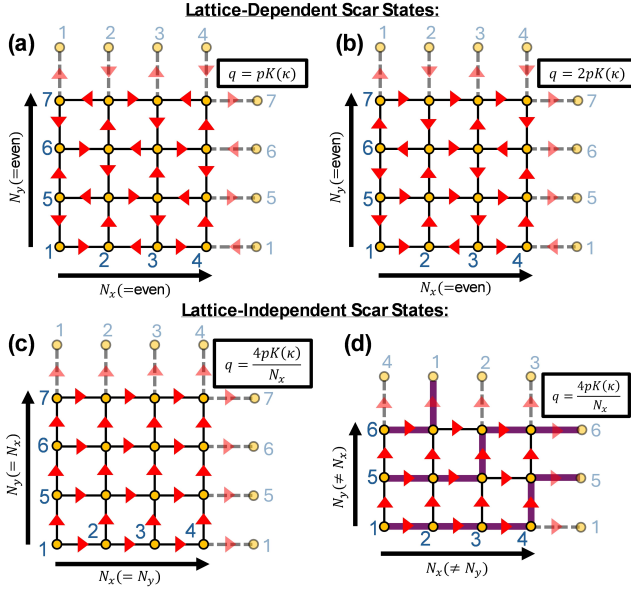


FIG. 4. (a) and (b) depicts the lattice-dependent scar states which have plaquette-dependent and size-independent  $q$ -values given by  $q = 4pK(\kappa)/N_l$ , where  $N_l = N'_p, N'_p - 2, \dots$ . In general,  $N_p$  is the number of edges in the smallest and  $p$  is an integer. (c) and (d) illustrates the lattice-independent scar states which have plaquette-independent and size-dependent  $q$ -values given by  $q = 4pK(\kappa)/N_\alpha$ , where  $\alpha$  denotes any direction  $x$  or  $y$  in case  $N_x = N_y$ , or it is the direction perpendicular to the direction of shifted boundary condition in case  $N_x \neq N_y$ .

sponding to the Eq. 24 qualifies as a scar state only if the following conditions are satisfied,

- (i) **Vertex rule:** For any vertex  $n$ , we have  $\sum_m \sigma_{nm} = 0$ , where the summation is over all the vertices adjacent to vertex  $n$ .
- (ii) **Circuit rule:** Any circuit  $\Gamma$  must satisfy  $\sum_{(n,m) \in \Gamma} \sigma_{nm} q = 0 \pmod{4K(\kappa)}$ , where  $K(\kappa)$  is the elliptic integral of first kind. A circuit  $\Gamma$  is a path in a graph that starts and ends at the same vertex.

The vertex rule can be visualized by assigning a direction to each edge, representing the value  $\sigma_{nm}$  associated with it (see Fig. 3(a), (b)). The outgoing arrow from the vertex  $n$  towards the adjacent vertex  $m$  represents  $\sigma_{nm} = +1$ , while an ingoing arrow from the vertex  $n$  to  $m$  represents  $\sigma_{nm} = -1$ . The vertex condition  $\sum_m \sigma_{nm} = 0$  literally means that the number of ingoing and outgoing arrows at each vertex must be equal. Additionally, the underlying physics of the vertex rule holds true because the  $z$ -component of the spin current must be zero for the scar state,

$$\langle \dot{S}_n^z \rangle = -\alpha\beta S^2 \text{dn}(q_n, \kappa) \text{sn}(q, \kappa) \sum_m \sigma_{nm} = 0, \quad (25)$$

where the summation is over the adjacent vertices of vertex  $n$ .

Sl. No.	Type of Lattice	Lattice-dependent scar state	Lattice-independent scar state
(I)	Odd Coordination number (e.g. honeycomb, Shastry-Sutherland)	✗	✗
(II)	Even Coordination number and Plaquette with odd edges (e.g. triangular, kagome)	✓	✗
(III)	Even Coordination number and Plaquette with even edges (e.g. square, Lieb)	✓	✓ or ✗

TABLE I. This table summarizes the possible types of scar states for different types of spatially uniform 2D lattices with centro-symmetric spin-exchange interaction. The last cell contains both check and cross marks, indicating that a type-(III) lattice is a necessary condition for realizing lattice-independent scars but not a sufficient one.

On the other hand, the circuit rule is a consequence of the uniqueness of the spin state at each vertex. A circuit path  $\Gamma$  connects vertex  $n$  to itself; therefore, the total change in the spin direction along the closed path must be zero, and the required condition is,

$$\sum_{(n,m) \in \Gamma} \sigma_{nm} q = 0 \pmod{4K(\kappa)}, \quad (26)$$

where  $K(\kappa)$  is the complete elliptic integral for eccentricity  $\kappa$ . The visualization of the circuit rule for different graphs is depicted in Fig. 3(c) and (d).

## B. Uniform 2D Lattices

In this section, we describe the construction of GZ scars on 2D lattices with NN CSSE interactions. Firstly, not all lattices can support such scar states due to the vertex law. This law requires each vertex to be connected to an even number of edges. As a result, only certain lattices with even coordination numbers—such as square, triangular, kagome, and Lieb—are valid candidates. In contrast, lattices like honeycomb and Shastry-Sutherland do not satisfy this criterion and are therefore unsuitable. However, the coordination number of a lattice can be modified to an even value by adding additional bonds, thereby making the lattice suitable for hosting GZ scar states (see Appendix. D).

We examine scar states on different lattices with toroidal boundary conditions and demonstrate that scar states can be classified into two categories: lattice-dependent and lattice-independent scar states. The  $q$ -values of lattice-dependent scars are limited to  $q = 4pK(\kappa)/N_l$ , where  $N_l$  can take values of  $N_p, N_p - 2, \dots$  and  $p$  is an integer. Here  $N_p$  is the number of edges of a plaquette, where a plaquette is defined as a closed circuit that does not cross the periodic boundaries. In general, the  $N_p$  corresponds to the smallest plaquette of a lattice. For square, Lieb, triangular, and kagome lattices,  $N_p$  takes values of 4, 8, 3 and 3 respectively (see Appendix. D). Fig. 4(a) and (b) demonstrate two types of lattice-dependent scar states on a square lattice with



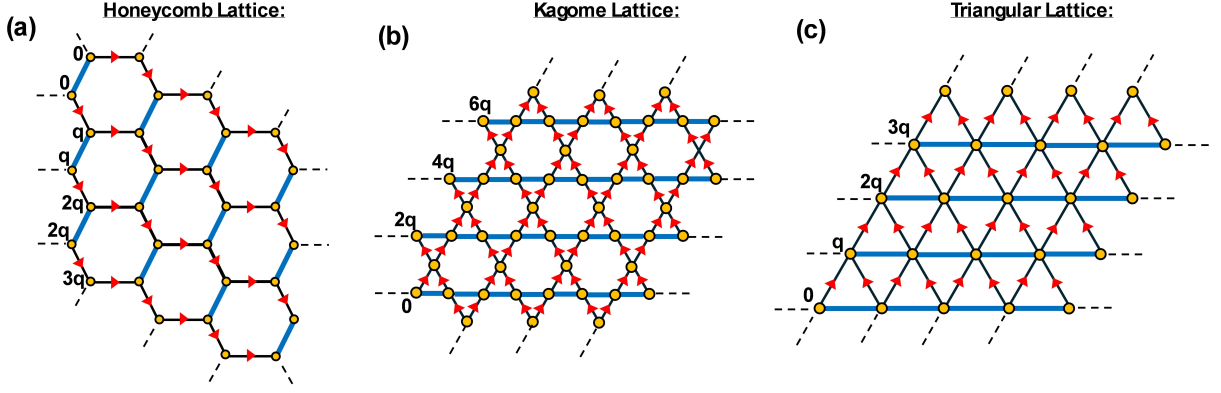


FIG. 5. Demonstration of lattice-independent GZ scars on (a) honeycomb lattice, (b) kagome lattice, and (c) triangular lattice. Spins connected by black (blue) bonds interact via a centrosymmetric (isotropic) Heisenberg exchange interaction. The red arrowhead denotes  $\sigma_{nm} = +1$ , whereas the  $\sigma_{nm} = 0$  on the blue bonds. The  $q$ -values for some of the boundary sites are shown for reference.

$N_l = 4$  and  $N_l = 2$  respectively. It is also noticeable that the  $q$ -values are independent of lattice dimension  $N_x \times N_y$ . The lattice-independent scar states can exhibit a range of  $q$ -values that do not depend on the lattice plaquette but rather on the system's size and shape. Figures 4(c) and (d) illustrate lattice-independent scar states on a square lattice, with (c) showing a system where the number of sites along the  $x$  and  $y$  directions is equal ( $N_x = N_y$ ), and (d) depicting a system with an unequal number of sites in these directions ( $N_x \neq N_y$ ). The  $q$ -value of these scars are  $q = 4pK(\kappa)/N_x$ . Noticeably, in the case of unequal lattice dimension ( $N_x \neq N_y$ ), a twisted or shifted boundary condition is required along one of the periodic boundaries to preserve the circuit law, as demonstrated by the purple circuit in Fig. 4(d). The shift in shifted boundary condition equals  $|N_x - N_y|$ . Furthermore, the  $q$ -value in such cases is  $q = 4pK(\kappa)/N_\alpha$ , where  $\alpha$  is the direction perpendicular to the direction of the shifted boundary condition.

A lattice-independent scar state satisfies a strict circuit rule,  $\sum_{(n,m) \in \Gamma} \sigma_{nm} q = 0$  on each plaquette  $\Gamma$ . Furthermore, this condition holds only when each plaquette has an even number of edges. Thus, the triangular and kagome lattices, which contain plaquettes with three edges, are unsuitable for hosting lattice-independent scar states. Although a lattice with all even plaquettes is a necessary condition for lattice-independent scars, it is not sufficient, as it does not guarantee a strict circuit rule on all the plaquettes simultaneously (see the example of modified honeycomb lattice in Appendix D). Based on our findings, we have summarized which types of lattices can or cannot host scar states and whether they support lattice-dependent or lattice-independent scar states in the Table I. Moreover, scar states can also be constructed in higher dimensions in a similar manner.

### C. Irregular 2D Lattices

In the previous subsection, we show that lattice-independent scars are only possible in the non-frustrated lattice models with even coordination number. However, this statement holds only when considering a spatially uniform lattice with a single type of CSSE interaction on NN bonds, with a Hamiltonian of the form given in Eq. 23. This subsection demonstrates that, given a CSSE Hamiltonian with certain bonds retaining full isotropic  $SU(2)$  symmetry, it is still possible to construct lattice-independent scar states on a frustrated lattice with odd coordination number. This is demonstrated in Fig. 5. The explicit expression of the Hamiltonian of such a system is,

$$\hat{H} = \sum_{(m,n) \in \mathcal{B}_1} \left[ J^x \hat{S}_m^x \hat{S}_n^x + J^y \hat{S}_m^y \hat{S}_n^y + J^z \hat{S}_m^z \hat{S}_n^z \right] + \sum_{(m,n) \in \mathcal{B}_2} J' \hat{\mathbf{S}}_m \cdot \hat{\mathbf{S}}_n, \quad (27)$$

where the bonds  $\mathcal{B}_1$  and  $\mathcal{B}_2$  are the blue and black bonds in Fig. 5. The value of  $q$  and  $\kappa$  of the scar state can be determined using Eq. 5. Moreover, the direction of the red arrow indicates  $\sigma_{nm} = +1$ , while its absence corresponds to  $\sigma_{nm} = 0$ . It can be observed that removing the blue bonds in Fig. 5 transforms the honeycomb, kagome, and triangular lattices into spin chains, the Lieb lattice, and the square lattice, respectively, which are the allowed lattices to have the lattice-independent scar states according to the table I. Therefore, the structure of the scar states in the models discussed here is intrinsically linked to NN CSSE systems that support lattice-independent scars. This approach can be further extended to lattices with isotropic Heisenberg exchange interactions on trimers, as illustrated in the Appendix D.

## V. DISCUSSION

In summary, we show various aspects of GZ scars, which have been overlooked by the physics community for more than three decades and have been re-introduced in a few works very recently. Although the concept of quantum scars—originally introduced by Heller in the context of single-particle systems—emerged around that time, their existence in many-body systems is a much more recent discovery. This zero-entangled scar state is especially intriguing, as it exhibits a periodicity significantly larger than that of the unit cell, despite the spatial uniformity of the Hamiltonian. In this work, we aim to understand the origin of such a surprising scar state through the lens of modern developments in scar state construction, which have emerged over the past decade. The existence of such scar states is rooted in the presence of a thermodynamically large degeneracy—i.e., a degeneracy that scales with the system size. We further show that this degenerate scar subspace possesses an underlying structure, which is relatively simple to describe in the case of helical scars in the XXZ limit but significantly more complex for GZ scars in the XYZ limit. This contrast arises from the fact that the helical scar subspace exhibits a quasi- $U(1)$  symmetry, which is absent in the GZ scar subspace. Due to this quasi- $U(1)$  symmetry, the helical scar subspace can be effectively described using the standard spectrum-generating algebra (SGA). Moreover, the XXZ Hamiltonian admits an  $\hat{H}_0 + \sum_a \hat{O}_a \hat{T}_a$  group-theoretical structure, allowing the helical scar subspace to be reinterpreted as a set of bosonic  $\zeta$ -states. In contrast, the absence of quasi- $U(1)$  symmetry in the XYZ limit makes the structure of the GZ scar subspace harder to capture. To address this, we propose two complementary approaches—approximated SGA and generalized SGA—to construct and describe the GZ scar subspace. Interestingly, the span of the GZ scar subspace with a given helicity is significantly larger than that of the helical scar subspace with the same helicity. This observation implies that the GZ scar subspace is not simply a deformed version of the helical scar subspace. However, due to the large overlap between the two, GZ scar states can still be well described using the helical scar subspace.

We further demonstrate that GZ scars are not limited to one-dimensional lattices; they can also be constructed in higher-dimensional lattices by following specific graphical rules, referred to as the vertex rule and the circuit rule. Using these rules, we identify uniform two-dimensional lattices with nearest-neighbor CSSE interactions that are capable of hosting lattice-independent GZ scars. Here, a lattice-independent scar is defined as a scar state whose  $q$ -value does not depend on the lattice type. Lattices with an even coordination number and plaquettes having an even number of edges, such as the square and Lieb lattices, can host lattice-independent scars. On the other hand, lattices such as the honeycomb, kagome, triangular, and Shastry–Sutherland lattices are not suitable for hosting lattice-independent scar states.

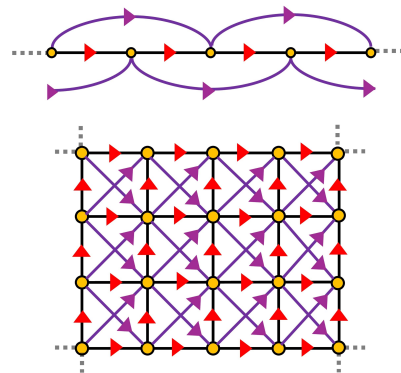


FIG. 6. Examples of GZ scars for fine-tuned Hamiltonians. The next-nearest neighbour one-dimensional spinchain (top figure) and two-dimensional square lattice (bottom figure) is shown. Along the red (purple) arrowheads  $\sigma_{nm} = +1$  ( $+2$ ). For such scar states, the Hamiltonian needs to be fine-tuned which means that the interaction parameters of the Hamiltonian need to be very specific and correlated with respect to each other. In these examples, the spin-exchange interaction parameters on the next-nearest neighbour bonds have to be fixed based on the interaction parameters on the nearest-neighbour bonds.

However, we also show that if certain bonds retain a fully  $SU(2)$ -symmetric Heisenberg exchange interaction, lattices such as the triangular, kagome, and honeycomb lattices become capable of hosting lattice-independent GZ scars.

While investigating scar-state construction on two-dimensional lattices, we deliberately avoid fine-tuned Hamiltonians tailored to support GZ scars. For example, a generic Hamiltonian of the following form contains GZ scars with a particular  $q$ -value,

$$\hat{H} = \sum_{\mathcal{B}_r} \sum_{(m,n) \in \mathcal{B}_r} J_r [\text{dn}(rq, \kappa) \hat{S}_m^x \hat{S}_n^x + \hat{S}_m^y \hat{S}_n^y + \text{cn}(rq, \kappa) \hat{S}_m^z \hat{S}_n^z], \quad (28)$$

where the summation is over different bonds  $\mathcal{B}_r$  and each of these bonds is associated with a  $q$ -value integer multiple of  $q$  such that the vertex rule and the circuit rule of resultant scar states are satisfied. We provided an example of such GZ scar constructions on such systems in Fig. 6. Although this construction yields a lattice-independent GZ scar state, it requires a highly fine-tuned Hamiltonian, making it of limited practical interest. Therefore, rather than beginning with a GZ scar state and determining the corresponding fine-tuned Hamiltonian, we adopt an alternative approach: Given a spin-exchange Hamiltonian with bonds that respect either centro-symmetry or  $SU(2)$  symmetry, we investigate whether a lattice-independent GZ scar state can emerge. The answer is affirmative; we find that a variety of two-dimensional lattices—including square, Lieb, kagome, triangular, and honeycomb—are all capable of hosting GZ scar states under these symmetry conditions.

*Acknowledgments.*— D. B. extends special thanks to Vir B. Bhulchandani for his valuable insights and discussions. D. B. also gratefully acknowledges Wai-Keong (Dariel) Mok and Daniel K. Mark for their thought-provoking conversations. W. W. H. is supported by

the National Research Foundation (NRF), Singapore, through the NRF Fellowship NRF-NRFF15-2023-0008, and through the National Quantum Office, hosted in A\*STAR, under its Centre for Quantum Technologies Funding Initiative (S24Q2d0009).

## Appendix A: Unitary Equivalence of Generic Centrosymmetric and XYZ Hamiltonians

This section shows how to transform a generic nearest-neighbor centrosymmetric Hamiltonian into the XYZ Hamiltonian step by step. We start with the following generic Hamiltonian in the lab frame with basis  $(1, 2, 3)$ ,

$$\mathcal{H} = \sum_n \left[ J_1 \hat{S}_n^1 \hat{S}_{n+1}^1 + J_2 \hat{S}_n^2 \hat{S}_{n+1}^2 + J_3 \hat{S}_n^3 \hat{S}_{n+1}^3 + J_{12} \left( \hat{S}_n^1 \hat{S}_{n+1}^2 + \hat{S}_n^2 \hat{S}_{n+1}^1 \right) \right. \\ \left. + J_{13} \left( \hat{S}_n^1 \hat{S}_{n+1}^3 + \hat{S}_n^3 \hat{S}_{n+1}^1 \right) + J_{13} \left( \hat{S}_n^1 \hat{S}_{n+1}^3 + \hat{S}_n^3 \hat{S}_{n+1}^1 \right) \right], \quad (\text{A1})$$

**Step 1:** We apply the following unitary transformations consecutively on the spin operators,

$$\hat{S}_n^\alpha \rightarrow \exp \left( -i\psi \hat{S}_n^x \right) \hat{S}_n^{\beta''} \exp \left( i\psi \hat{S}_n^x \right), \quad \hat{S}_n^{\beta''} \rightarrow \exp \left( -i\phi \hat{S}_n^y \right) \hat{S}_n^{\beta'} \exp \left( i\phi \hat{S}_n^y \right), \quad (\text{A2})$$

where,  $\alpha \in (1, 2, 3)$ ,  $\beta' \in (x', y', z')$ ,  $\beta'' \in (x'', y'', z'')$

which are equivalent to the following  $SO(3)$  transformations respectively,

$$\begin{pmatrix} \hat{S}_n^1 \\ \hat{S}_n^2 \\ \hat{S}_n^3 \end{pmatrix} \rightarrow \underbrace{\begin{pmatrix} 1 & 0 & 0 \\ 0 & \cos(\psi) & -\sin(\psi) \\ 0 & \sin(\psi) & \cos(\psi) \end{pmatrix}}_{R_x(\psi)} \begin{pmatrix} \hat{S}_n^{x'} \\ \hat{S}_n^{y'} \\ \hat{S}_n^{z'} \end{pmatrix}, \quad \begin{pmatrix} \hat{S}_n^1 \\ \hat{S}_n^2 \\ \hat{S}_n^3 \end{pmatrix} \rightarrow \underbrace{\begin{pmatrix} \cos(\phi) & 0 & \sin(\phi) \\ 0 & 1 & 0 \\ -\sin(\phi) & 0 & \cos(\phi) \end{pmatrix}}_{R_y(\phi)} \begin{pmatrix} \hat{S}_n^{x'} \\ \hat{S}_n^{y'} \\ \hat{S}_n^{z'} \end{pmatrix}. \quad (\text{A3})$$

Using the transformations Eq. A3 into the Hamiltonian Eq. A1, we get,

$$\mathcal{H} = \sum_n \left[ J'_x \hat{S}_n^{x'} \hat{S}_{n+1}^{x'} + J'_y \hat{S}_n^{y'} \hat{S}_{n+1}^{y'} + J'_z \hat{S}_n^{z'} \hat{S}_{n+1}^{z'} + J'_{xy} \left( \hat{S}_n^{x'} \hat{S}_{n+1}^{y'} + \hat{S}_n^{y'} \hat{S}_{n+1}^{x'} \right) \right], \quad (\text{A4})$$

where the magnitudes of the exchange interactions are,

$$\begin{aligned} J'_x &= J_1 \cos^2(\phi) + J_2 \sin^2(\phi) \sin^2(\psi) + J_3 \sin^2(\phi) \cos^2(\psi) + J_{12} \sin(2\phi) \sin(\psi) \\ &\quad + J_{13} \sin(2\phi) \cos(\psi) + J_{23} \sin^2(\phi) \sin(2\psi) \\ J'_y &= J_2 \cos^2(\psi) + J_3 \sin^2(\psi) - J_{23} \sin(2\psi) \\ J'_z &= J_1 \sin^2(\phi) + J_2 \cos^2(\phi) \sin^2(\psi) + J_3 \cos^2(\phi) \cos^2(\psi) - J_{12} \sin(2\phi) \sin(\psi) \\ &\quad - J_{13} \sin(2\phi) \cos(\psi) + J_{23} \cos^2(\phi) \sin(2\psi) \\ J'_{xy} &= J_{12} \cos(\phi) \cos(\psi) - J_{13} \cos(\phi) \sin(\psi) + J_{23} \sin(\phi) \cos(2\psi) + \frac{1}{2} (J_2 - J_3) \sin(\phi) \sin(2\psi), \end{aligned} \quad (\text{A5})$$

and to determine the variables  $\psi$  and  $\phi$ , we have to solve the following equations numerically,

$$\begin{aligned} [J_{13} \sin(\psi) - J_{12} \cos(\psi)] \sin(\phi) + \left[ \frac{1}{2} (J_2 - J_3) \sin(2\psi) - J_{23} \cos(2\psi) \right] \cos(\phi) &= 0 \\ \frac{\sin(2\phi)}{2} [-J_1 + J_2 \sin^2(\psi) + J_3 \cos^2(\psi)] + [J_{12} \sin(\psi) + J_{13} \cos(\psi)] \cos(2\phi) + \frac{1}{2} J_{23} \sin(2\psi) \sin(2\phi) &= 0 \end{aligned} \quad (\text{A6})$$

**Step 2:** The generated Hamiltonian after Step 1 is Eq. A4, which we rewrite here,

$$\mathcal{H} = J'_x \hat{S}_n^{x'} \hat{S}_{n+1}^{x'} + J'_y \hat{S}_n^{y'} \hat{S}_{n+1}^{y'} + J'_z \hat{S}_n^{z'} \hat{S}_{n+1}^{z'} + J'_{xy} \left( \hat{S}_n^{x'} \hat{S}_{n+1}^{y'} + \hat{S}_n^{y'} \hat{S}_{n+1}^{x'} \right). \quad (\text{A7})$$

This Hamiltonian is further connected with XYZ Hamiltonian,

$$\mathcal{H} = \sum_n \left[ J_x \hat{S}_n^x \hat{S}_{n+1}^x + J_y \hat{S}_n^y \hat{S}_{n+1}^y + J_z \hat{S}_n^z \hat{S}_{n+1}^z \right], \quad (\text{A8})$$

via the following unitary transformation,

$$\hat{S}_n^\beta \rightarrow \exp(-i\theta \hat{S}_n^z) \hat{S}_n^\gamma, \text{ where, } \beta \in (x', y', z'), \gamma \in (x, y, z), \quad (\text{A9})$$

which is equivalent to the following  $SO(3)$  transformation,

$$\begin{pmatrix} \hat{S}_n^{x'} \\ \hat{S}_n^{y'} \\ \hat{S}_n^{z'} \end{pmatrix} \rightarrow \underbrace{\begin{pmatrix} \cos(\theta) & -\sin(\theta) & 0 \\ \sin(\theta) & \cos(\theta) & 0 \\ 0 & 0 & 1 \end{pmatrix}}_{R_z(\theta)} \begin{pmatrix} \hat{S}_n^x \\ \hat{S}_n^y \\ \hat{S}_n^z \end{pmatrix}, \text{ where, } \theta = \frac{1}{2} \tan^{-1} \left( \frac{2J'_{xy}}{J'_x - J'_y} \right) \quad (\text{A10})$$

The coefficients of Hamiltonian A7 and A8 are related as,

$$\begin{aligned} J_x &= \frac{1}{2}(J'_x + J'_y) \pm \sqrt{(J'_x - J'_y)^2 + 4(J'_{xy})^2} \\ J_y &= \frac{1}{2}(J'_x + J'_y) \mp \sqrt{(J'_x - J'_y)^2 + 4(J'_{xy})^2} \\ J_z &= J'_z \end{aligned} \quad (\text{A11})$$

**Summary:** So we perform three  $SO(3)$  rotations,

$$\begin{aligned} (1, 2, 3) &\xrightarrow{R_x^{-1}(\psi)} (x'', y'', z''), \\ (x'', y'', z'') &\xrightarrow{R_y^{-1}(\phi)} (x', y', z'), \\ (x', y', z') &\xrightarrow{R_z^{-1}(\theta)} (x, y, z) \end{aligned} \quad (\text{A12})$$

The  $SO(3)$  matrices  $(R_x(\psi), R_y(\phi), R_z(\theta))$  are given in the equations A3 and A10. The angles  $\psi$  and  $\phi$  are determined by solving Equation A6, while the expression of  $\theta$  is,

$$\theta = \frac{1}{2} \tan^{-1} \left( \frac{2J'_{xy}}{J'_x - J'_y} \right), \quad (\text{A13})$$

where, The coefficients  $J'_x, J'_y, J'_{xy}$  are given in equation Eq. A5.

## Appendix B: Proof of Granovskii-Zhedanov Scar

The proof of the existence of the periodic scar state in XYZ Hamiltonian is provided by Granovskii and Zhedanov. For the sake of completeness and the reader's convenience, we reproduce the proof here.

First, we transform the Hamiltonian unitarily so that the Granovskii-Zhedanov scar state becomes an all-up state in the rotated frame,

$$|\uparrow\rangle = \prod_n \exp(i\hat{S}_n^z \phi_n) \exp(i\hat{S}_n^y \theta_n) |\Psi_{GZ}\rangle. \quad (\text{B1})$$

The expressions of  $\phi_n$  and  $\theta_n$  are given in Eq. 3. This also transforms the spin operators as,

$$\begin{pmatrix} \hat{S}_n^x \\ \hat{S}_n^y \\ \hat{S}_n^z \end{pmatrix} = \begin{pmatrix} -N_n \text{sn}(w_n, \kappa) & -N_n \text{sn}(\bar{w}_n, \kappa) & \alpha \text{cn}(nq, \kappa) \\ N_n \text{cn}(w_n, \kappa) & N_n \text{cn}(\bar{w}_n, \kappa) & \beta \text{sn}(nq, \kappa) \\ iN_n & -iN_n & \gamma \text{dn}(nq, \kappa) \end{pmatrix} \begin{pmatrix} \hat{S}_n^+ \\ \hat{S}_n^- \\ \hat{S}_n^z \end{pmatrix}, \quad (\text{B2})$$



where  $w_n = nq + iv$  and  $v$  is the incomplete elliptic integral of the first kind with elliptic modulus  $k' = \sqrt{1 - k^2}$  and  $N_n = \sqrt{1 - \gamma^2 \operatorname{dn}^2(nq, \kappa)}$ .  $q$  is an arbitrary parameter, and in this section, we derive its relation to the exchange coefficients. XYZ Hamiltonian after the transformation becomes,

$$\mathcal{H}' = \sum_n [\mathcal{C}_n^{--} \hat{s}_n^- \hat{s}_{n+1}^- + \mathcal{C}_n^{-+} \hat{s}_n^- \hat{s}_{n+1}^+ + \mathcal{C}_n^{-z} \hat{s}_n^- \hat{s}_{n+1}^z + \mathcal{C}_n^{z-} \hat{s}_n^z \hat{s}_{n+1}^- + \text{H.C.}] + \mathcal{C}_n^{zz} \hat{s}_n^z \hat{s}_{n+1}^z, \quad (\text{B3})$$

where the coefficients are given by,

$$\begin{aligned} \mathcal{C}_n^{--} &= N_n N_{n+1} [J_x \operatorname{sn}(\bar{w}_n, \kappa) \operatorname{sn}(\bar{w}_{n+1}, \kappa) + J_y \operatorname{cn}(\bar{w}_n, \kappa) \operatorname{cn}(\bar{w}_{n+1}, \kappa) - J_z] \\ \mathcal{C}_n^{-+} &= N_n N_{n+1} [J_x \operatorname{sn}(\bar{w}_n) \operatorname{sn}(w_{n+1}) + J_y \operatorname{cn}(\bar{w}_n) \operatorname{cn}(w_{n+1}) + J_z] \\ \mathcal{C}_n^{-z} &= -N_n [J_x \alpha \operatorname{sn}(\bar{w}_n) \operatorname{cn}(nq + q) - J_y \beta \operatorname{cn}(\bar{w}_n) \operatorname{sn}(nq + q) + i J_z \gamma \operatorname{dn}(nq + q)] \\ \mathcal{C}_n^{z-} &= -N_{n+1} [J_x \alpha \operatorname{cn}(nq) \operatorname{sn}(\bar{w}_{n+1}) - J_y \beta \operatorname{sn}(nq) \operatorname{cn}(\bar{w}_{n+1}) + i J_z \gamma \operatorname{dn}(nq)] \\ \mathcal{C}_n^{zz} &= [J_x \alpha^2 \operatorname{cn}(nq) \operatorname{cn}(nq + q) + J_y \beta^2 \operatorname{sn}(nq) \operatorname{sn}(nq + q) + J_z \gamma^2 \operatorname{dn}(nq) \operatorname{dn}(nq + q)]. \end{aligned} \quad (\text{B4})$$

If the state  $|\Psi\rangle_{GZ}$  is a scar state of the XYZ Hamiltonian, then the following eigenvalue equation must be satisfied,

$$\begin{aligned} \mathcal{H}' |\uparrow\rangle &= E |\uparrow\rangle \\ \Rightarrow \sum_n [\{\mathcal{C}_n^{--} \hat{s}_n^- \hat{s}_{n+1}^- + \mathcal{C}_n^{-+} \hat{s}_n^- \hat{s}_{n+1}^+ + \mathcal{C}_n^{-z} \hat{s}_n^- \hat{s}_{n+1}^z + \mathcal{C}_n^{z-} \hat{s}_n^z \hat{s}_{n+1}^- + \text{H.C.}\} + \mathcal{C}_n^{zz} \hat{s}_n^z \hat{s}_{n+1}^z] |\uparrow\rangle &= E |\uparrow\rangle \\ \Rightarrow \sum_n [\mathcal{C}_n^{--} \hat{s}_n^- \hat{s}_{n+1}^- + \mathcal{C}_n^{-z} \hat{s}_n^- \hat{s}_{n+1}^z + \mathcal{C}_n^{z-} \hat{s}_n^z \hat{s}_{n+1}^- + \mathcal{C}_n^{zz} \hat{s}_n^z \hat{s}_{n+1}^z] |\uparrow\rangle &= E |\uparrow\rangle \\ \Rightarrow \sum_n [\mathcal{C}_n^{--} \hat{s}_n^- \hat{s}_{n+1}^- + S \mathcal{C}_n^{-z} \hat{s}_n^- + S \mathcal{C}_n^{z-} \hat{s}_{n+1}^- + S^2 \mathcal{C}_n^{zz}] |\uparrow\rangle &= E |\uparrow\rangle \\ \Rightarrow \sum_n [\mathcal{C}_n^{--} \hat{s}_n^- \hat{s}_{n+1}^- + S (\mathcal{C}_n^{-z} + \mathcal{C}_{n-1}^{z-}) \hat{s}_n^- + S^2 \mathcal{C}_n^{zz}] |\uparrow\rangle &= E |\uparrow\rangle. \end{aligned} \quad (\text{B5})$$

To be a valid eigen equation, the following conditions must be satisfied,

$$\mathcal{C}_n^{--} = 0 \quad \text{and} \quad \mathcal{C}_n^{-z} + \mathcal{C}_{n-1}^{z-} = 0. \quad (\text{B6})$$

This condition holds if,

$$\operatorname{dn}(q, \kappa) = \frac{J_x}{J_y}, \quad \operatorname{cn}(q, \kappa) = \frac{J_z}{J_y}, \quad (\text{B7})$$

and it can be proved by using the following identities,

$$\begin{aligned} \operatorname{cn}(a, \kappa) \operatorname{cn}(b, \kappa) + \operatorname{dn}(a - b, \kappa) \operatorname{sn}(a, \kappa) \operatorname{sn}(b, \kappa) - \operatorname{cn}(a - b, \kappa) &= 0 \\ \operatorname{dn}(a - b, \kappa) \operatorname{sn}(a, \kappa) \operatorname{cn}(b, \kappa) - \operatorname{cn}(a, \kappa) \operatorname{sn}(b, \kappa) - \operatorname{dn}(a, \kappa) \operatorname{sn}(a - b, \kappa) &= 0. \end{aligned} \quad (\text{B8})$$

## Appendix C: Scar Subspace

### 1. Degeneracy of Scar Subspace

To understand the origin of such the GZ scar, we study the spectral degeneracy at the energy of the GZ scar,

$$E_{GZ} = N S^2 \operatorname{cn}(q, \kappa) \operatorname{dn}(q, \kappa) + k^2 \operatorname{sn}^2(q, \kappa) \sum_n \operatorname{sn}(nq, \kappa) \operatorname{sn}(nq + q, \kappa). \quad (\text{C1})$$

We perform exact diagonalization of the spin system using the QuSpin Python package[76]. By leveraging the translational and spin-flip symmetries, we aim to diagonalize the largest possible system size. The numerical data are tabulated in Fig. 7, and we further analyze the degeneracy pattern as a function of system size, as presented in the table. Apart from special cases such as  $S = 1/2$  and  $q$ -values that are integer multiples of  $K(\kappa)$ , the degeneracy of the scar subspace is observed to be  $4NS$ . This finding further supports the analysis presented in the main text.

$S = 1/2, q = 4K(\kappa)/2$		
System Length(N)	Degeneracy (D)	Estimate
2	3	$D = N + 1$
4	5	
6	7	
8	9	
10	11	
12	13	
14	15	
16	17	
18	19	

$S = 1, q = 4K(\kappa)/2$		
System Length(N)	Degeneracy (D)	Estimate
2	5	$D = 2N + 1$
4	9	
6	13	
8	17	
10	21	
12	25	

$S = 3/2, q = 4K(\kappa)/2$		
System Length(N)	Degeneracy (D)	Estimate
2	7	$D = 3N + 1$
4	13	
6	19	
8	25	

$S = 1/2, q = 4K(\kappa)/3$		
System Length(N)	Degeneracy (D)	Estimate
3	6	$D = 3 \times 2^{\lfloor \frac{N}{3} \rfloor}$
6	12	
9	24	
12	48	
15	96	
18	192	

$S = 1, q = 4K(\kappa)/3$		
System Length(N)	Degeneracy (D)	Estimate
3	12	$D = 4N$
6	24	
9	36	
12	48	

$S = 3/2, q = 4K(\kappa)/3$		
System Length(N)	Degeneracy (D)	Estimate
3	18	$D=6N$
6	36	
9	54	

FIG. 7. Degeneracy of the energy level corresponding to the GZ scar, calculated using exact diagonalization technique for several spin and  $q$ -values. It is observed that the degeneracy generally increases linearly with the system size, except for  $S = 1/2$  or  $q = 4K(\kappa)/2$ , where the integrability of the model causes deviations from this trend.

## 2. Spectrum Generating Algebra (SGA) in XXZ limit

Moreover, in the main text, we described the scar state in the XXZ limit using spectrum generating algebra (SGA). In this appendix, we elaborate on it. Suppose,  $\hat{H}$  is the XXZ Hamiltonian, then it satisfies the following commutation relation with generator  $\hat{\tau}$ ,

$$[\hat{H}, \hat{\tau}] = \hat{\Lambda}, \quad \text{with } \hat{\tau} = \sum_n e^{inq} \hat{S}_n^- \quad \text{and} \quad \hat{\Lambda} = i \sin(q) \sum_n e^{inq} \hat{S}_n^- [\hat{S}_{n+1}^z - \hat{S}_{n-1}^z]. \quad (\text{C2})$$

Additionally, it can be shown that the following relations also hold,

$$[\hat{\tau}, \hat{\Lambda}] = 0, \quad \hat{\Lambda} |\uparrow\rangle = 0, \quad \hat{H} |\uparrow\rangle = E_{GZ} |\uparrow\rangle \quad (\text{C3})$$

Using the above equations we can show that the state  $|\mathcal{S}^{(m)}\rangle = \hat{\tau}^m |\uparrow\rangle$  is also eigenstate of  $\mathcal{H}$ , as follows,

$$\begin{aligned}
\hat{H} |\mathcal{S}^{(m)}\rangle &= \hat{H} \hat{\tau}^m |\uparrow\rangle \\
&= [\hat{\tau} \hat{H} + \hat{\Lambda}] \hat{\tau}^{m-1} |\uparrow\rangle \\
&= [\hat{\tau} \hat{H} \hat{\tau}^{m-1} + \hat{\tau}^{m-1} \hat{\Lambda}] |\uparrow\rangle \\
&= \hat{\tau} \hat{H} \hat{\tau}^{m-1} |\uparrow\rangle \quad \left[ \hat{\Lambda} |\uparrow\rangle = 0 \right] \\
&\vdots \\
&= \hat{\tau}^m \hat{H} |\uparrow\rangle \\
&= E_{GZ} \hat{\tau}^m |\uparrow\rangle
\end{aligned}$$

### 3. generalized SGA using small $\gamma$ expansion

In the main text, we demonstrate that the generalized SGA for the GZ scar subspace can be generated using rotation operators. However, this is not the only possible set of operators that defines the generalized SGA. Here, we show that expanding the rotation operator in a Taylor series with respect to the free parameter  $\gamma$  yields an alternative set of operators that also define a generalized SGA. The generating operators obtained in this manner can be used to construct the scar states (up to a normalization constant) as follows,

$$\begin{aligned} |\mathcal{S}^{(m)}\rangle &= \hat{\mathcal{T}}^{(m)} |\uparrow'\rangle, \text{ with} \\ |\uparrow'\rangle &= \prod_n e^{-i \tan^{-1} \text{sc}(nq, \kappa) \hat{S}_n^z} e^{-i \frac{\pi}{2} \hat{S}_n^y} |\uparrow\rangle. \end{aligned} \quad (\text{C4})$$

The generating operators  $\hat{\mathcal{T}}^{(p)}$  can be obtained from the small- $\gamma$  expansion of the rotation operator  $\hat{\mathcal{R}}$  in Eq. 4 defined in main text. This involves collecting the coefficient operators of the  $\gamma^p$  term and applying a unitary transformation to them. The unitary transformation corresponds to the transformation of  $|\uparrow\rangle$  to  $|\uparrow'\rangle$  defined in the above equation. While these operators can be generated numerically, we provide analytical expressions for completeness, which facilitate more efficient numerical computations. The generating operators are given by,

$$\hat{\mathcal{T}}^{(p)} = \sum_{\substack{\alpha, \beta, \dots \\ N\text{-term}}}^{(p)} \hat{\mathcal{C}}_{1, \alpha} \hat{\mathcal{C}}_{2, \beta} \dots \quad (\text{C5})$$

Here, the indices  $1, 2, \dots$  label lattice sites, and the summation with superscript  $(p)$  indicates that the indices  $q, r, \dots$  are whole numbers that sum to  $p$ . The operators  $\hat{\mathcal{C}}_{n, p}$  can be further expressed as,

$$\hat{\mathcal{C}}_{n, p} = \sum_{q=0}^p \hat{W}_{n, \alpha}^{(z)} \hat{W}_{n, p-\alpha}^{(y)}. \quad (\text{C6})$$

Here the operators  $\hat{W}_{n, p}^{(z)}$  and  $\hat{W}_{n, p}^{(y)}$  consist of strings of  $\hat{S}_n^z$  and  $\hat{S}_n^y$ , respectively. The rotated spin operators are,

$$\hat{S}_n^y = -\sin(q_n) \hat{S}_n^x + \cos(q_n) \hat{S}_n^y, \quad (\text{C7})$$

where  $q_n = \tan^{-1} \text{sc}(nq, \kappa)$ . The exact form of the operator  $\hat{W}_{n, p}^{(y)}$  is given by,

$$\begin{aligned} \hat{W}_{n, p}^{(y)} &= (\text{dn}(nq, \kappa))^p \sum_{m \in \mathbb{S}_p} \frac{(i \hat{S}_n^y)^m}{4^{(\frac{p-m}{2})}} \\ &\times \sum_{\substack{\alpha, \beta, \dots \\ m\text{-terms}}}^{(\frac{p-m}{2})} \frac{(2\alpha)!(2\beta)! \dots}{(\alpha!)^2 (2\alpha+1) \cdot (\beta!)^2 (2\beta+1) \dots}, \end{aligned} \quad (\text{C8})$$

where the superscript over the sum indicates that the variables are whole number that sum to  $\frac{p-m}{2}$  and the set  $\mathbb{S}_p$  is a set of odd (even) number ranging from 1 to  $p$  given that  $p$  is odd (even). The approximate form of operator  $\hat{W}_{n, p}^{(x)}$  for small  $\kappa$  is given by,

$$\begin{aligned} \hat{W}_{n, p}^{(z)} &= \hat{\mathbb{I}}, \text{ for } p = 0 \\ &= -i \frac{\kappa^2 \text{sc}(nq, \kappa)}{2(1 + \text{sc}^2(nq, \kappa))} \hat{S}_n^z, \text{ for even } p \\ &= 0, \text{ for odd } p, \end{aligned} \quad (\text{C9})$$

The exact  $\hat{W}_{n, p}^{(z)}$  operators are only non-zero for even indices  $p$  and have the following form,

$$\hat{W}_{n, p}^{(z)} = \sum_{m=1}^{p/2} \frac{(-i \hat{S}_n^z)^m}{m!} \sum_{\substack{\alpha, \beta, \dots \\ m\text{-terms}}}^{(p/2)} c_{n, \alpha} c_{n, \beta} \dots, \quad (\text{C10})$$

where the indices of primed summation with superscript  $(p/2)$  is runs from 1 to  $(p/2)$  with a constraint  $\alpha + \beta + \dots = p/2$ . The coefficients  $c_{n,p}$  can be obtained iteratively from recursive equations. The coefficients  $c_{n,p}$  are basically the coefficients of the following Taylor-series expansion,

$$\tan^{-1} \left( \frac{a_n \sqrt{1-m'x}}{\sqrt{1-x}} \right) = \sum_{p=0}^{\infty} c_{n,p} x^p, \quad (C11)$$

where,  $x = \gamma^2$ ,  $m' = 1 - k^2$ ,  $a_n = \text{sc}(nq, \kappa)$ . The coefficients are,

$$c_{n,0} = \tan^{-1}(a_n), \quad c_{n,1} = \frac{a_n}{2} \frac{1-m'}{1+a_n^2}$$

$$c_{n,p} = \frac{1}{4p} \left[ (p-1)(y_{p+3}^{(1)} + y_{p+3}^{(2)}) + (p-1)(y_{p+4}^{(3)} + y_{p+4}^{(4)}) - (p-2)(y_{p+4}^{(5)} + y_{p+4}^{(6)}) \right], \quad (C12)$$

where  $y_p^{(i)}$  can be determined by solving the following difference equations iteratively. The variables  $y_p^{(1)}$  and  $y_p^{(2)}$  can be obtained by solving the following recursive equation,

$$y_{n+3}^{(i)} = \frac{1}{2(p+3)(1+a_n^2)} \left[ 2m'(1+p)(1+a_n^2 m') y_n^{(i)} + (9+3a_n^2+5m'+11a_n^2 m'+2p(2+a_n^2+m'+2a_n^2 m')) y_{n+2}^{(i)} \right. \\ \left. + (-3-2p-7m'-4pm'-5a_n^2 m'-4pa_n^2 m'-5a_n^2 m'^2-2pa_n^2 m'^2) y_{n+1}^{(i)} \right]. \quad (C13)$$

The initial values for  $y_p^{(1)}$  and  $y_p^{(2)}$  are,

$$y_0^{(1)} = \frac{ia_n m'}{a_n - i}, \quad y_1^{(1)} = \frac{a_n m'(1+m'+2ia_n m')}{2(a_n - i)^2}$$

$$y_2^{(1)} = \frac{a_n m'}{8(a_n - i)^3} (-3i + a_n - 2im' + 6a_n m' + 6a_n m' - 3im'^2 + 9a_n m'^2 + 8ia_n^2 m'^2)$$

$$y_0^{(2)} = \left( y_0^{(1)} \right)^*, \quad y_1^{(2)} = \left( y_1^{(1)} \right)^*, \quad y_2^{(2)} = \left( y_2^{(1)} \right)^*, \quad (C14)$$

The variables  $y_p^{(3)}$ ,  $y_p^{(4)}$ ,  $y_p^{(5)}$  and  $y_p^{(6)}$  can be determined by using following recursive equation,

$$y_{n+4}^{(i)} = \frac{1}{2(p+4)(1+a_n^2)} \left[ 2m'(2+p)(1+a_n^2 m') y_n^{(i)} \right. \\ \left. + (-5-2p-15m'-6pm'-9a_n^2 m'-4pa_n^2 m'-11a_n^2 m'^2-4pa_n^2 m'^2) y_{n+1}^{(i)} \right. \\ \left. + (18+5a_n^2+18m'-6pm'-9a_n^2 m'-4pa_n^2 m'-11a_n^2 m'^2-4pa_n^2 m'^2) y_{n+2}^{(i)} \right. \\ \left. + (-21-6p-13a_n^2-4pa_n^2-7m'-2pm'-15a_n^2 m'-4pa_n^2 m') y_{n+3}^{(i)} \right]. \quad (C15)$$

The initial values for  $y_p^{(3)}$ ,  $y_p^{(4)}$ ,  $y_p^{(5)}$  and  $y_p^{(6)}$  are,

$$y_0^{(3)} = \frac{-ia_n}{i-a_n}, \quad y_1^{(3)} = \frac{a_n}{2} \frac{-3-2ia_n-m'-2ia_n m'}{(a_n-i)^2},$$

$$y_2^{(3)} = \frac{-ia_n}{8(a_n-i)^3} (-15-21ia_n+8a_n^2-6m'-18ia_n m'+8a_n^2 m'-3m'^2-9ia_n m'^2+8a_n^2 m'^2)$$

$$y_3^{(3)} = \frac{a_n}{16(a_n-i)^4} (35+76ia_n-59a_n^2-16ia_n^3+15m'+60ia_n m'-55a_n^2 m'-16ia_n^3 m'+9m'^2+36ia_n m'^2-49a_n^2 m'^2 \\ -16ia_n^3 m'^2+5m'^3+20ia_n m'^3-29a_n^2 m'^3-16ia_n^3 m'^3),$$

$$y_0^{(4)} = \left( y_0^{(3)} \right)^*, \quad y_1^{(4)} = \left( y_1^{(3)} \right)^*, \quad y_2^{(4)} = \left( y_2^{(3)} \right)^*, \quad y_3^{(4)} = \left( y_3^{(3)} \right)^*$$

$$y_0^{(5)} = m' y_0^{(3)}, \quad y_1^{(5)} = m' y_1^{(3)}, \quad y_2^{(5)} = m' y_2^{(3)}, \quad y_3^{(5)} = m' y_3^{(3)}$$

$$y_0^{(6)} = m' \left( y_0^{(3)} \right)^*, \quad y_1^{(6)} = m' \left( y_1^{(3)} \right)^*, \quad y_2^{(6)} = m' \left( y_2^{(3)} \right)^*, \quad y_3^{(6)} = m' \left( y_3^{(3)} \right)^* \quad (C16)$$



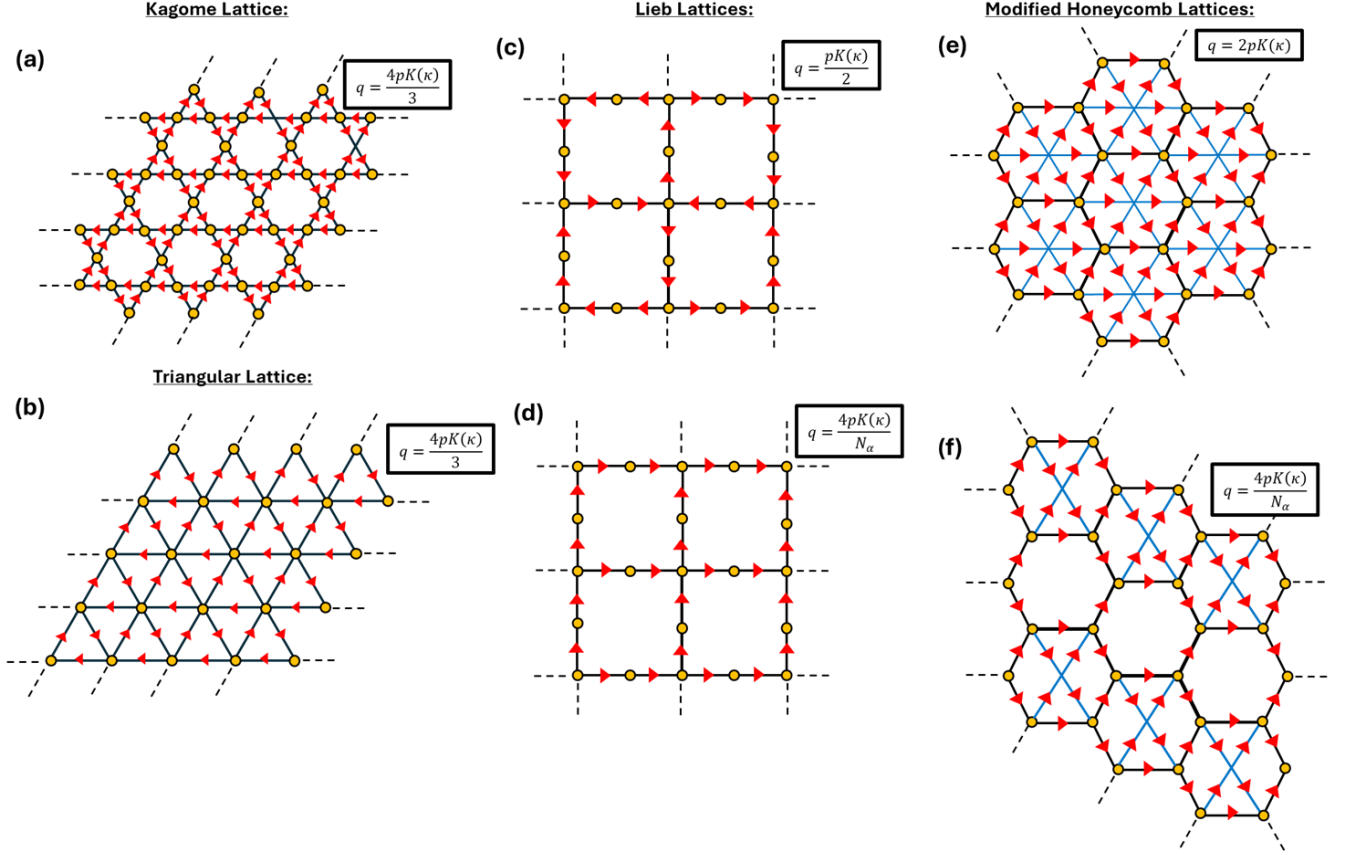


FIG. 8. (a) and (b) represents lattice-dependent scar states on kagome and triangular lattice, respectively. (c) and (d) illustrate lattice-dependent and lattice-independent scar states on Lieb lattice, respectively. (e) and (f) depict the lattice-dependent and lattice-independent scar states on modified honeycomb lattices, respectively.

#### 4. Deformation Operators

We check for the suitable spin-1/2 deforming operators that deform the  $SU(2)$  scar subspace to  $U(1)$  scar subspace. The type-1 and the type-2 deforming operators are defined by [73],

$$W_{\text{type-1}} = a |\uparrow\rangle \langle\uparrow| + b |\downarrow\rangle \langle\downarrow|, \quad W_{\text{type-2}} = \begin{pmatrix} a |\uparrow\rangle \langle\uparrow| + b |\downarrow\rangle \langle\downarrow| & e \hat{\sigma}^+ \\ f \hat{\sigma}^- & c |\uparrow\rangle \langle\uparrow| + d |\downarrow\rangle \langle\downarrow| \end{pmatrix}. \quad (\text{C17})$$

These deforming operators leave the fully-polarized state  $|\uparrow\rangle$  unchanged. Since  $|\uparrow\rangle$  is not a basis state of the scar subspace in the XYZ case, these operators are not suitable for deforming the scar subspace. Thus the only remaining option for the deforming operator is the type-3 deforming operator,

$$W_{\text{type-3}} = \begin{pmatrix} a |\uparrow\rangle \langle\uparrow| & c \hat{\sigma}^+ \\ d |\uparrow\rangle \langle\uparrow| & b |\downarrow\rangle \langle\downarrow| \end{pmatrix} \quad (\text{C18})$$

This is also not a suitable deforming operator as it annihilates the  $|\uparrow\rangle$  state. However, the deformation must happen adiabatically such that there must be a scar state in the XYZ case correspond to  $|\uparrow\rangle$  state in the XYZ limit. Thus there are no suitable deforming operator that deforms the  $SU(2)$  scar subspace of the XXZ Hamiltonian to describe the GZ scar subspace as a  $U(1)$  scar subspace.

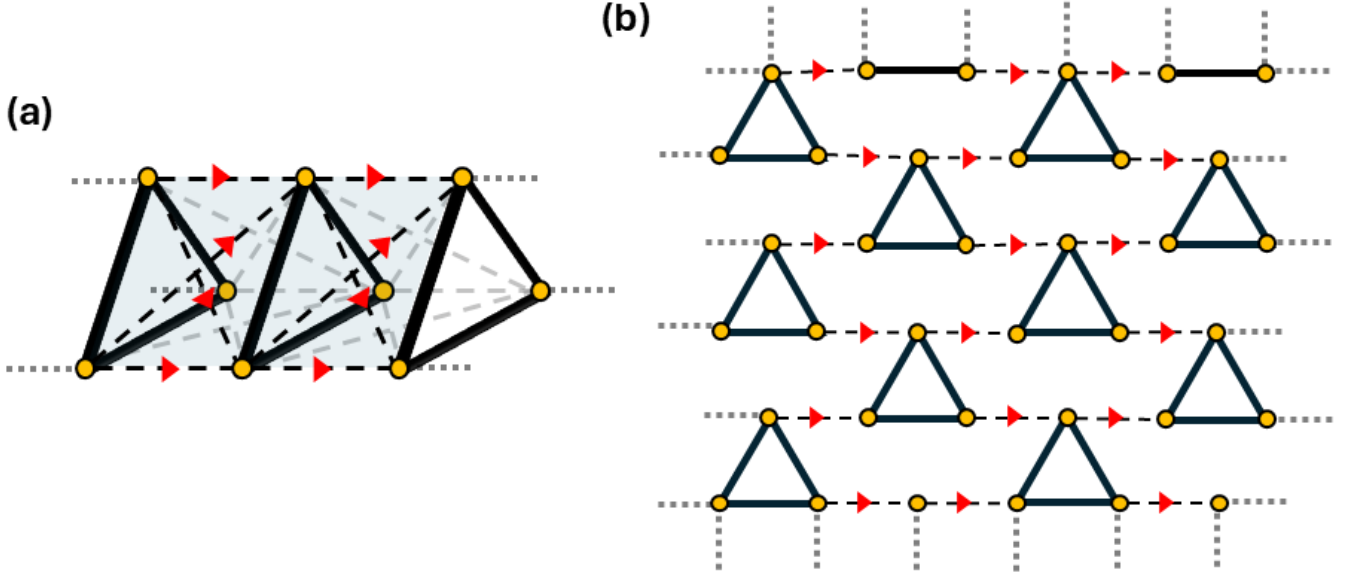


FIG. 9. (a) Trimer spin-ladder model. (b) Trimer brick wall lattice model. The spins connected by thick black bonds interact via an isotropic Heisenberg exchange interaction, while those connected by dashed black bonds interact via an XYZ-like spin-exchange interaction. Red arrowheads indicate a change in the  $q$ -value.

## Appendix D: Lattice-Dependent and Lattice-Independent Scars in Various nearest-neighbor 2D Lattices

### 1. Uniform Lattices

This section demonstrates the construction of scar state on various lattices. The only possible scar states for the uniform triangular and kagome lattices are lattice-dependent due to the presence of triangular plaquettes with an odd number of edges (see Fig. 8(a), (b)). On the other hand, the Lieb lattice can host both lattice-dependent and lattice-independent scar states, as shown in Fig. 8(c) and (d). Although the uniform honeycomb lattice, in principle, cannot host any scar states due to its odd coordination number (three), it can be modified to accommodate scar states by adding additional nearest neighbor bonds to achieve an even coordination number. As we show in Fig. 8(e) and (f), the modified honeycomb lattice can host both lattice-dependent and lattice-independent scar states.

### 2. Irregular Lattices with trimers

In the main text, we show that incorporating  $SU(2)$ -invariant bonds into lattices such as triangular, kagome, and honeycomb enables the introduction of lattice-independent GZ scars in these systems. In this appendix, we demonstrate that the concept can be further generalized to the frustrated trimer lattices. Fig. 9 illustrates two different types of trimer lattices, where thick black bonds ( $\mathcal{B}_D$ ) form the trimers, and dashed bonds ( $\mathcal{B}_d$ ) connect them. The Hamiltonian of these trimer systems is,

$$\hat{H} = J \sum_{(m,n) \in \mathcal{B}_D} \hat{\mathbf{S}}_m \cdot \hat{\mathbf{S}}_n + J' \sum_{(m,n) \in \mathcal{B}_d} \left[ \text{dn}(q, \kappa) \hat{S}_m^x \hat{S}_n^x + \hat{S}_m^y \hat{S}_n^y + \text{cn}(q, \kappa) \hat{S}_m^z \hat{S}_n^z \right]. \quad (\text{D1})$$

Red arrowheads in the Fig. 9 visually represent the GZ scar. Interestingly, no arrowheads appear on the trimer bonds  $\mathcal{B}_D$ , since their  $q$ -value remains constant. The vertex and circuit rules continue to hold.

- 
- [1] J. v. Neumann, *Beweis des Ergodensatzes und des H-Theorems in der neuen Mechanik*, *Z. Physik* **57**, 30 (1929).
- [2] J. v. Neumann, *Proof of the ergodic theorem and the H-theorem in quantum mechanics*, *Z. Physik* **35**, 201 (2010).
- [3] J. M. Deutsch, *Quantum statistical mechanics in a closed system*, *Phys. Rev. A* **43**, 2046 (1991).
- [4] M. Srednicki, *Chaos and quantum thermalization*, *Phys. Rev. E* **50**, 888 (1994).
- [5] M. Srednicki, *Thermal fluctuations in quantized chaotic systems*, *Journal of Physics A: Mathematical and General* **29**, L75 (1996).
- [6] M. Rigol, V. Dunjko, and M. Olshanii, *Thermalization and its mechanism for generic isolated quantum systems*, *Nature* **452**, 854 (2008).
- [7] L. D'Alessio, Y. Kafri, A. Polkovnikov, and M. R. and, *From quantum chaos and eigenstate thermalization to statistical mechanics and thermodynamics*, *Advances in Physics* **65**, 239 (2016).
- [8] J. M. Deutsch, *Eigenstate thermalization hypothesis*, *Rep. Prog. Phys.* **81**, 082001 (2018).
- [9] M. Srednicki, *The approach to thermal equilibrium in quantized chaotic systems*, *Journal of Physics A: Mathematical and General* **32**, 1163 (1999).
- [10] R. Nandkishore and D. A. Huse, *Many-Body Localization and Thermalization in Quantum Statistical Mechanics*, *Annual Review of Condensed Matter Physics* **6**, 15 (2015).
- [11] D. A. Abanin, E. Altman, I. Bloch, and M. Serbyn, *Colloquium: Many-body localization, thermalization, and entanglement*, *Rev. Mod. Phys.* **91**, 021001 (2019).
- [12] C. J. Turner, A. A. Michailidis, D. A. Abanin, M. Serbyn, and Z. Papić, *Weak ergodicity breaking from quantum many-body scars*, *Nature Physics* **14**, 745 (2018).
- [13] C. J. Turner, A. A. Michailidis, D. A. Abanin, M. Serbyn, and Z. Papić, *Quantum scarred eigenstates in a Rydberg atom chain: Entanglement, breakdown of thermalization, and stability to perturbations*, *Phys. Rev. B* **98**, 155134 (2018).
- [14] S. Dooley, *Robust Quantum Sensing in Strongly Interacting Systems with Many-Body Scars*, *PRX Quantum* **2**, 020330 (2021).
- [15] H.-R. Wang, D. Yuan, S.-Y. Zhang, Z. Wang, D.-L. Deng, and L.-M. Duan, *Embedding Quantum Many-Body Scars into Decoherence-Free Subspaces*, *Phys. Rev. Lett.* **132**, 150401 (2024).
- [16] W. W. Ho, S. Choi, H. Pichler, and M. D. Lukin, *Periodic Orbits, Entanglement, and Quantum Many-Body Scars in Constrained Models: Matrix Product State Approach*, *Phys. Rev. Lett.* **122**, 040603 (2019).
- [17] V. Khemani, C. R. Laumann, and A. Chandran, *Signatures of integrability in the dynamics of Rydberg-blockaded chains*, *Phys. Rev. B* **99**, 161101 (2019).
- [18] S. Choi, C. J. Turner, H. Pichler, W. W. Ho, A. A. Michailidis, Z. Papić, M. Serbyn, M. D. Lukin, and D. A. Abanin, *Emergent  $SU(2)$  Dynamics and Perfect Quantum Many-Body Scars*, *Phys. Rev. Lett.* **122**, 220603 (2019).
- [19] M. Serbyn, D. A. Abanin, and Z. Papić, *Quantum many-body scars and weak breaking of ergodicity*, *Nature Physics* **17**, 675 (2021).
- [20] Z. Papić, *Weak ergodicity breaking through the lens of quantum entanglement*, (2021), [arXiv:2108.03460](https://arxiv.org/abs/2108.03460) [cond-mat.quant-gas].
- [21] Q. Chen, S. A. Chen, and Z. Zhu, *Weak ergodicity breaking in non-Hermitian many-body systems*, *SciPost Phys.* **15**, 052 (2023).
- [22] R. Shen, F. Qin, J.-Y. Desaulles, Z. Papić, and C. H. Lee, *Enhanced Many-Body Quantum Scars from the Non-Hermitian Fock Skin Effect*, *Phys. Rev. Lett.* **133**, 216601 (2024).
- [23] A. J. A. James, R. M. Konik, and N. J. Robinson, *Non-thermal States Arising from Confinement in One and Two Dimensions*, *Phys. Rev. Lett.* **122**, 130603 (2019).
- [24] N. J. Robinson, A. J. A. James, and R. M. Konik, *Signatures of rare states and thermalization in a theory with confinement*, *Phys. Rev. B* **99**, 195108 (2019).
- [25] O. Vafek, N. Regnault, and B. A. Bernevig, *Entanglement of exact excited eigenstates of the Hubbard model in arbitrary dimension*, *SciPost Phys.* **3**, 043 (2017).
- [26] T. Iadecola and M. Žnidarič, *Exact Localized and Ballistic Eigenstates in Disordered Chaotic Spin Ladders and the Fermi-Hubbard Model*, *Phys. Rev. Lett.* **123**, 036403 (2019).
- [27] D. K. Mark and O. I. Motrunich,  *$\eta$ -pairing states as true scars in an extended Hubbard model*, *Phys. Rev. B* **102**, 075132 (2020).
- [28] S. Moudgalya, N. Regnault, and B. A. Bernevig,  *$\eta$ -pairing in Hubbard models: From spectrum generating algebras to quantum many-body scars*, *Phys. Rev. B* **102**, 085140 (2020).
- [29] S. Moudgalya, B. A. Bernevig, and N. Regnault, *Quantum many-body scars in a Landau level on a thin torus*, *Phys. Rev. B* **102**, 195150 (2020).
- [30] B. Nachtergaele, S. Warzel, and A. Young, *Low-complexity eigenstates of a  $\nu = 1/3$  fractional quantum Hall system*, *Journal of Physics A: Mathematical and Theoretical* **54**, 01LT01 (2020).
- [31] S. Pai and M. Pretko, *Dynamical Scar States in Driven Fracton Systems*, *Phys. Rev. Lett.* **123**, 136401 (2019).
- [32] S. Ok, K. Choo, C. Mudry, C. Castelnovo, C. Chamon, and T. Neupert, *Topological many-body scar states in dimensions one, two, and three*, *Phys. Rev. Res.* **1**, 033144 (2019).
- [33] N. Shiraishi, *Connection between quantum-many-body scars and the Affleck-Kennedy-Lieb-Tasaki model from the viewpoint of embedded Hamiltonians*, *Journal of Statistical Mechanics: Theory and Experiment* **2019**, 083103 (2019).
- [34] S. Moudgalya, N. Regnault, and B. A. Bernevig, *Entanglement of exact excited states of Affleck-Kennedy-Lieb-Tasaki models: Exact results, many-body scars, and violation of the strong eigenstate thermalization hypothesis*, *Phys. Rev. B* **98**, 235156 (2018).
- [35] D. K. Mark, C.-J. Lin, and O. I. Motrunich, *Unified structure for exact towers of scar states in the Affleck-Kennedy-Lieb-Tasaki and other models*, *Phys. Rev. B* **101**, 195131 (2020).
- [36] S. Moudgalya, E. O'Brien, B. A. Bernevig, P. Fendley, and N. Regnault, *Large classes of quantum scarred Hamiltonians from matrix product states*, *Phys. Rev. B* **102**, 085120 (2020).

- [37] M. Schechter and T. Iadecola, *Weak Ergodicity Breaking and Quantum Many-Body Scars in Spin-1 XY Magnets*, *Phys. Rev. Lett.* **123**, 147201 (2019).
- [38] S. Chattopadhyay, H. Pichler, M. D. Lukin, and W. W. Ho, *Quantum many-body scars from virtual entangled pairs*, *Phys. Rev. B* **101**, 174308 (2020).
- [39] K. Lee, R. Melendrez, A. Pal, and H. J. Changlani, *Exact three-colored quantum scars from geometric frustration*, *Phys. Rev. B* **101**, 241111 (2020).
- [40] P. A. McClarty, M. Haque, A. Sen, and J. Richter, *Disorder-free localization and many-body quantum scars from magnetic frustration*, *Phys. Rev. B* **102**, 224303 (2020).
- [41] A. Chandran, T. Iadecola, V. Khemani, and R. Moessner, *Quantum Many-Body Scars: A Quasiparticle Perspective*, *Annual Review of Condensed Matter Physics* **14**, 443 (2023).
- [42] S. Moudgalya, B. A. Bernevig, and N. Regnault, *Quantum many-body scars and Hilbert space fragmentation: a review of exact results*, *Reports on Progress in Physics* **85**, 086501 (2022).
- [43] I. Lee, F. G. Utermohlen, D. Weber, K. Hwang, C. Zhang, J. van Tol, J. E. Goldberger, N. Trivedi, and P. C. Hammel, *Fundamental Spin Interactions Underlying the Magnetic Anisotropy in the Kitaev Ferromagnet CrI<sub>3</sub>*, *Phys. Rev. Lett.* **124**, 017201 (2020).
- [44] C. Peng, S. Mardanya, A. N. Petsch, V. K. Sharma, S. Li, C. Jia, A. Bansil, S. Chowdhury, and J. J. Turner, *Kitaev physics in the two-dimensional magnet NiPSe<sub>3</sub>*, *Phys. Rev. Res.* **6**, 033206 (2024).
- [45] H. Suzuki, H. Liu, J. Bertinshaw1, K. Ueda1, H. Kim1, S. Laha, D. Weber, Z. Yang1, L. Wang, H. Takahashi, K. Fürsich, M. Minola, B. V. Lotsch, B. J. Kim, H. Yavaş, M. Daghofer, J. Chaloupka, G. Khaliullin, H. Gretarsson, and B. Keimer, *Proximate ferromagnetic state in the Kitaev model material  $\alpha$ -RuCl<sub>3</sub>*, *Nat. Commun.* **12**, 4512 (2021).
- [46] W. Lu, J. Tuchendler, M. von Ortenberg, and J. P. Renard, *Direct observation of the Haldane gap in NENP by far-infrared spectroscopy in high magnetic fields*, *Phys. Rev. Lett.* **67**, 3716 (1991).
- [47] W. Lu, J. Tuchendler, M. von Ortenberg, and J. P. Renard, *Haldane topological spin-1 chains in a planar metal-organic framework*, *Nat. Commun.* **14**, 5454 (2023).
- [48] M. E. Zayed, C. Rüegg, J. Larrea, A. M. Läuchli7, C. Panagopoulos, S. S. Saxena8, M. Ellerby5, D. F. McMorro5, T. Strässle, S. Klotz10, G. Hamel10, R. A. Sadykov, V. Pomjakushin, M. Boehm13, M. Jiménez-Ruiz13, A. Schneidewind, E. Pomjakushina, M. Stingaciu, K. Conder, and H. Rønnow, *4-spin plaquette singlet state in the Shastry–Sutherland compound SrCu<sub>2</sub>(BO<sub>3</sub>)<sub>2</sub>*, *Nat. Phys.* **13**, 962 (2017).
- [49] H. Kageyama, K. Yoshimura, R. Stern, N. V. Mushnikov, K. Onizuka, M. Kato, K. Kosuge, C. P. Slichter, T. Goto, and Y. Ueda, *Exact Dimer Ground State and Quantized Magnetization Plateaus in the Two-Dimensional Spin System SrCu<sub>2</sub>(BO<sub>3</sub>)<sub>2</sub>*, *Phys. Rev. Lett.* **82**, 3168 (1999).
- [50] S. Murmann, F. Deuretzbacher, G. Zürn, J. Bjerlin, S. M. Reimann, L. Santos, T. Lompe, and S. Jochim, *Antiferromagnetic Heisenberg Spin Chain of a Few Cold Atoms in a One-Dimensional Trap*, *Phys. Rev. Lett.* **115**, 215301 (2015).
- [51] E. Rosenberg, T. I. Andersen, and R. Samajdar *et. al.*, *Dynamics of magnetization at infinite temperature in a Heisenberg spin chain*, *Science* **384**, 48–53 (2024).
- [52] P. N. Jepsen, J. Amato-Grill, I. Dimitrova, W. W. Ho, E. Demler, and W. Ketterle, *Spin transport in a tunable Heisenberg model realized with ultracold atoms*, *Nature* **588**, 403–407 (2020).
- [53] P. N. Jepsen, W. W. Ho, J. Amato-Grill, I. Dimitrova, E. Demler, and W. Ketterle, *Transverse Spin Dynamics in the Anisotropic Heisenberg Model Realized with Ultracold Atoms*, *Phys. Rev. X* **11**, 041054 (2021).
- [54] P. N. Jepsen, Y. K. Lee, H. Lin, I. Dimitrova, Y. Margalit, W. W. Ho, and W. Ketterle, *Long-lived phantom helix states in Heisenberg quantum magnets*, *Nature Physics* **18**, 899–904 (2022).
- [55] X. Zhang, A. Klümper, and V. Popkov, *Phantom Bethe roots in the integrable open spin- $\frac{1}{2}$  XXZ chain*, *Phys. Rev. B* **103**, 115435 (2021).
- [56] E. S. Ma, K. L. Zhang, and Z. Song, *Steady helix states in a resonant XXZ Heisenberg model with Dzyaloshinskii-Moriya interaction*, *Phys. Rev. B* **106**, 245122 (2022).
- [57] G. Zhang and Z. Song, *Stable dynamic helix state in the nonintegrable XXZ Heisenberg model*, *Physica Scripta* **99**, 075119 (2024).
- [58] V. Popkov, M. Žnidarič, and X. Zhang, *Universality in the relaxation of spin helices under XXZ spin-chain dynamics*, *Phys. Rev. B* **107**, 235408 (2023).
- [59] V. Popkov, J. Schmidt, and C. Presilla, *Spin-helix states in the XXZ spin chain with strong boundary dissipation*, *Journal of Physics A: Mathematical and Theoretical* **50**, 435302 (2017).
- [60] H.-R. Wang and D. Yuan, *Generalized Spin Helix States as Quantum Many-Body Scars in Partially Integrable Models*, (2024), [arXiv:2403.14755 \[quant-ph\]](https://arxiv.org/abs/2403.14755).
- [61] F. Gerken, I. Runkel, C. Schweigert, and T. Posske, *All product eigenstates in Heisenberg models from a graphical construction*, *Phys. Rev. Res.* **7**, L012008 (2025).
- [62] Y. I. Granovskii and A. Zhedanov, *Periodic structures on a quantum spin chain*, *Zh. Eksp. Teor. Fiz* **89**, 2156 (1985).
- [63] Y. I. Granovskii and A. S. Zhedanov, *Coherent structures in a Heisenberg anisotropic array*, *JETP Letters* **41**, 312 (1985).
- [64] E. J. Heller, *Bound-State Eigenfunctions of Classically Chaotic Hamiltonian Systems: Scars of Periodic Orbits*, *Phys. Rev. Lett.* **53**, 1515 (1984).
- [65] D. Bhowmick, V. B. Bulchandani, and W. W. Ho, *Asymmetric decay of quantum many-body scars in XYZ quantum spin chains*, (2025), [arXiv:2505.05435 \[quant-ph\]](https://arxiv.org/abs/2505.05435).
- [66] M. Zheng, C. Liang, S. Chen, and X. Zhang, *Exact spin helix eigenstates in anisotropic spin-s Heisenberg model in arbitrary dimensions*, (2025), [arXiv:2505.14994 \[math-ph\]](https://arxiv.org/abs/2505.14994).
- [67] Y. B. Shi and Z. Song, *Robust unidirectional phantom helix states in the XXZ Heisenberg model with Dzyaloshinskii-Moriya interaction*, *Phys. Rev. B* **108**, 085108 (2023).
- [68] K. Pakrouski, P. N. Pallegar, F. K. Popov, and I. R. Klebanov, *Many-Body Scars as a Group Invariant Sector of Hilbert Space*, *Phys. Rev. Lett.* **125**, 230602 (2020).
- [69] K. Pakrouski, P. N. Pallegar, F. K. Popov, and I. R. Klebanov, *Group theoretic approach to many-body scar states in fermionic lattice models*, *Phys. Rev. Res.* **3**, 043156 (2021).
- [70] S. Hild, T. Fukuhara, P. Schauß, J. Zeiher, M. Knap, E. Demler, I. Bloch, and C. Gross, *Far-from-Equilibrium*



- Spin Transport in Heisenberg Quantum Magnets*, [Phys. Rev. Lett. \*\*113\*\*, 147205 \(2014\)](#).
- [71] N. Shiraishi and T. Mori, *Systematic Construction of Counterexamples to the Eigenstate Thermalization Hypothesis*, [Phys. Rev. Lett. \*\*119\*\*, 030601 \(2017\)](#).
- [72] J. Ren, C. Liang, and C. Fang, *Quasisymmetry Groups and Many-Body Scar Dynamics*, [Phys. Rev. Lett. \*\*126\*\*, 120604 \(2021\)](#).
- [73] J. Ren, C. Liang, and C. Fang, *Deformed symmetry structures and quantum many-body scar subspaces*, [Phys. Rev. Res. \*\*4\*\*, 013155 \(2022\)](#).
- [74] C. Jonay and F. Pollmann, *Localized Fock Space Cages in Kinetically Constrained Models*, (2025), [arXiv:2504.20987 \[quant-ph\]](#).
- [75] T.-L. Tan and Y.-P. Huang, *Interference-caged quantum many-body scars: the Fock space topological localization and interference zeros*, (2025), [arXiv:2504.07780 \[cond-mat.str-el\]](#).
- [76] P. Weinberg and M. Bukov, *QuSpin: a Python package for dynamics and exact diagonalisation of quantum many body systems. Part II: bosons, fermions and higher spins*, [SciPost Phys. \*\*7\*\*, 020 \(2019\)](#).